Available online at www.sciencedirect.com
ScienceDirect
Trans. Nonferrous Met. Soc. China 32(2022) 1−44
Transactions of Nonferrous Metals Society of China
www.tnmsc.cn

Fabrication of titanium-based alloys with bioactive surface oxide layer as biomedical implants: Opportunity and challenges

Mohamad Rodzi SITI NUR HAZWANI, Ling Xin LIM, Zainovia LOCKMAN, Hussain ZUHAILAWATI

Biomaterials Niche Area Group, School of Materials and Mineral Resources Engineering, Universiti Sains Malaysia, Engineering Campus, 14300 Nibong Tebal, Penang, Malaysia

Received 23 February 2021; accepted 25 November 2021

Abstract: Titanium and its alloys have long been used as implant materials due to their outstanding mechanical properties and apparent biocompatibility. Despite this, the search for better alloys has continued to be active by researchers and industries alike, as there are still pressing issues that require attention. These include (1) a large mismatch in the elastic modulus of the implant material, which causes a stress shielding problem; (2) the release of harmful ions from Ti alloys after long-term use; (3) a low bioactivity of the Ti alloy surface, which prolongs the healing process. More research has been directed toward finding new generation Ti alloys composed of more biocompatible phases and modifying the surface of Ti alloys from naturally bio-inert to bioactive in order to circumvent the problems. This review examines recent work reported on the fabrication of Ti alloys, and based on the survey, major characteristics highlighted the importance of elastic modulus and the use of non-toxic metal elements to improve biocompatibility. In terms of surface modification of Ti alloys, numerous studies have found that a nano-scaled surface oxide layer grown on the surface is always beneficial to improving the bioactivity of Ti alloys for rapid recovery after implantation. This comprehensive review focuses on the appropriate phase and composition for new Ti alloys intended for use as biomedical implants, emphasizing both fabrication and surface modification methods.
Key words: titanium alloy; orthopedic application; surface modification; TiO_2 nanotubes

1 Introduction

The first titanium mineral, menachanite, was discovered in 1791 but started only in 1910, titanium has been applied in engineering fields including automotive and aviation industries, owing to its high strength and low-density properties. Ti can be alloyed to improve its properties even further. Since the 1960s, Ti and its alloys have been widely used as metallic biomaterials in a variety of biomedical applications, including cardiovascular, orthopaedic, dentistry, prosthesis, craniofacial, and joint replacement surgery [1].

Plates for internal fixation were first reported in 1895 [2]. Surgical stainless-steel (316L), cobalt-chromium (CoCr) alloys and Ti alloys have since then been extensively used in bone fracture fixation and angioplasty. These materials have good biocompatibility, long-term stability and excellent mechanical properties. Moreover, Ti and Ti alloys have also been used as permanent implants, especially as bone tissue implants, as they possess excellent biocompatibility, good osseointegration, superior corrosion resistance, mechanical integrity and good physicochemical stability. Nevertheless, not all Ti alloys are biocompatible to human body. Titanium−aluminum−vanadium alloy specifically Ti−6Al−4V is a well-established primary metallic biomaterial for orthopedic implants and has been used for many years; however, it is also known to display toxicity after being long term used, due to

Corresponding author: Hussain ZUHAILAWATI, Tel: +604-5995258, E-mail: zuhaila@usm.my
DOI: 10.1016/S1003-6326(21)65776-X

the release of aluminum and vanadium-associated ions [3].

A search for alternative Ti alloys and the best composition to replace this commercial alloy Ti−6Al−4V has remained active, not only to address toxicity issues, but also to overcome elastic modulus mismatch [4]. Several studies on the use of emerging new Ti alloys have been published, with the primary focus being on determining the best composition and phase. The potential alloying elements for new Ti alloys are aimed at lowering the elastic modulus, thus solving the mismatch problem, while not causing any toxicity. Moreover, the alloy must have corrosion resistance at par with that pure Ti [4]. The purpose of this review is to present current findings on suitable phase, composition, and fabrication for biocompatible Ti alloys.

Another critical issue with Ti and Ti alloys-based implants is the bio-inert nature of the metals, which does not support chemical connection to the bone to actively induce bone growth, also known as osseointegration. The implants remained as a foreign substance at the implantation sites, causing the healing process to be prolonged [3]. Since the biological response to biomaterial is primarily governed by the surface properties of the biomaterial, it is critical to engineer the surface of the implant material appropriately in order to achieve the desired surface interaction with the surrounding cells and proteins. One method for accomplishing this is to intentionally form surface oxide, which can also induce surface nano-structuring. Metal oxide is formed as a result of metal oxidation. Titanium oxide, titania, or TiO_2 can exist in a variety of phases, the most common of which is rutile titania. Oxidation can occur through a thermal, physical, or chemical process. This oxide layer, if fabricated with specific properties, can aid in the biological response of the implant material. As there are many new publications on this topic, this review focuses on the chemical-based surface modification methods for Ti and its alloys, specifically for biomaterial applications.

2 Alloying chemistry: Microstructure design

The primary goal in designing Ti alloys for implant applications is to reduce their elastic modulus. This strategy can be implemented by tailoring the microstructure of Ti, which is typically classified into four categories: pure α, near-α, α+β and β phase alloys. In terms of the four categories mentioned, Ti alloying elements fall into three major groups: α-stabilizers, β-stabilizers, or neutral. Figures 1 and 2 depict the phase transformations of

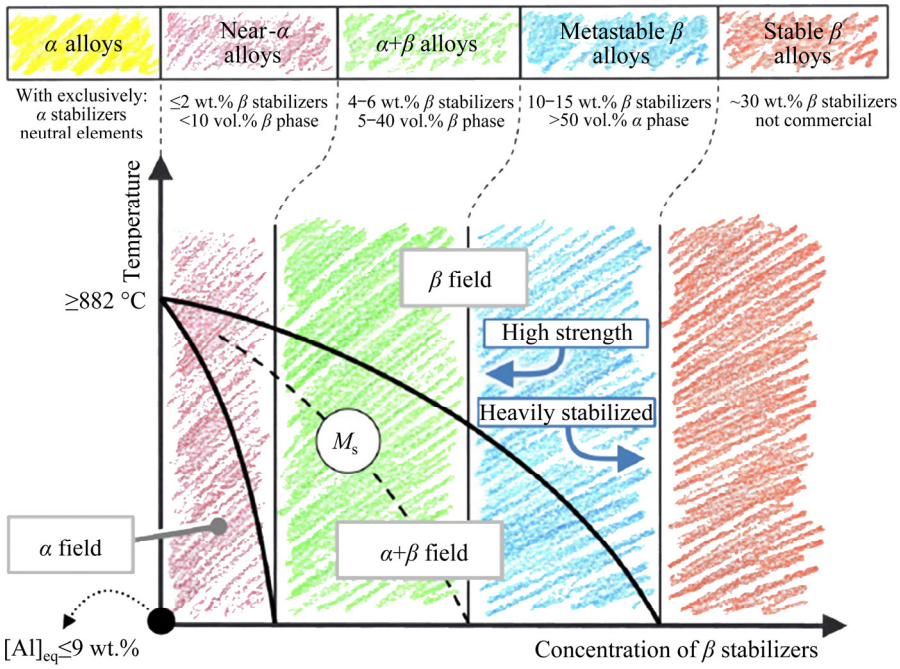

Fig. 1 Classification of titanium alloys (Reprinted with permission from Refs. [5−8]. Copyright 2015, Vienna University of Technology)

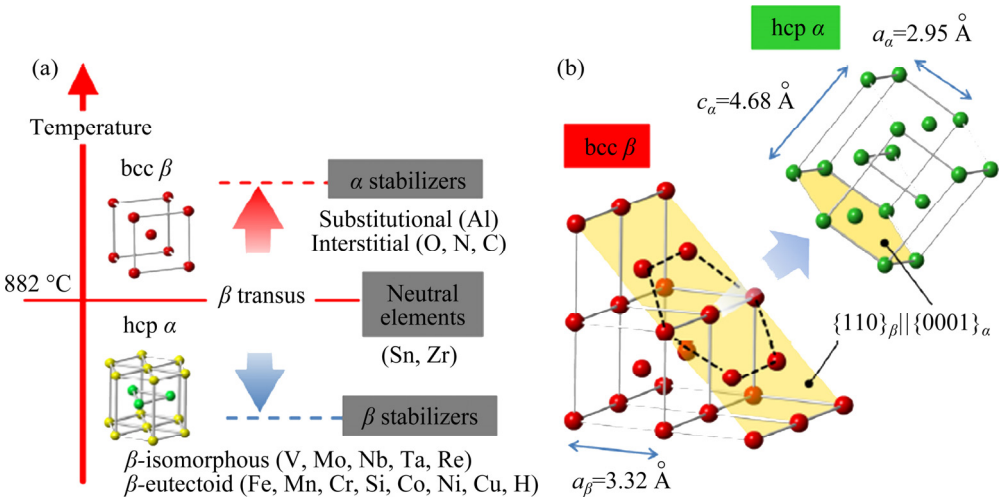

Fig. 2 Changes in crystal structure of Ti-based alloys based on alloying elements (a), and lattice correspondence between hcp-α and bcc-β structures (b) (The lattice parameters correspond to the values of pure titanium at room temperature and 900 °C. Reprinted with permission from Refs. [5−8]. Copyright 2015, Vienna University of Technology)

Ti alloys. Essentially, a crystallographic transformation of Ti occurs at 882 °C in pure Ti. This temperature is referred to as the β-transus temperature, T_β. Commercially pure Ti (cp-Ti) has a hexagonal close-packed (hcp) structure below this temperature, which is referred to as α-phase. Above 882 °C, a phase transformation occurs, in which hcp gradually transforms to a body-centered cubic (bcc) structure. This transformation typically generates a two-phase field with both α and β phases, and slowly forms only β phase with the increasing amount of β-stabilizer [1,9].

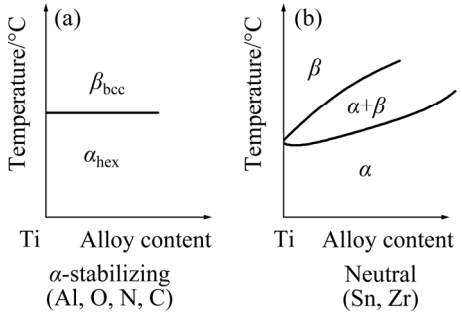

Fig. 3 Effect of α-stabilizing elements on Ti (a), and effect of neutral elements on Ti (b) (Reprinted with permission from Ref. [10]. Copyright 2013, Elsevier)

2.1 α and near-α Ti alloys

α-Ti alloys are composed of α-phase with the addition of α-stabilizers (such as Al, O, N, C, B) to Ti (Fig. 3(a)); whereas near-α alloys are composed of α-stabilizers, with less quantities of β-stabilizers (<5 wt.%) [1], but behave as conventional α alloys. This type of Ti-alloy is not heat treatable but has good weldability. Essentially, they have superior creep resistance and excellent corrosion resistance. To strengthen the α phase, tin (Sn) or zirconium (Zr) can be added, which has no effect on the transformation temperature and thus is referred to as neutral (Fig. 3(b)).

This α type of Ti alloy contains a major class of unalloyed titanium/commercially pure titanium that differ in the amount of O and Fe. Commercially pure Ti is also known as cp-Ti, which is a high purity alloy containing at least 99% pure titanium. There are various grades of cp-Ti. There are four grades of cp-Ti, all of which have a low content of interstitial elements such as Fe, O, N, and H. These interstitial elements promote the process of interstitial solid solution strengthening, which affects the mechanical properties of Ti alloy.

Mechanical strengths are typically limited and relatively low at room temperature for this α-type of alloy, and unfortunately, due to their hcp structure (very stable), these limitations of α-type Ti alloys cannot be improved by heat treatment. As a result, α-type Ti alloys are never a good choice for use as implants, whereas near-α Ti alloys have yet to be studied for their potential in biomedical applications.

2.2 (α+β)-Ti alloys

(α+β)-Ti alloys are a mixture of α and β phases,

with additions of α and β-stabilizers, but with a higher content of β-stabilizers (4−6 wt.%) (Fig. 1). Ti alloys of this type are heat-treatable and have good fabricability [11]. As a result, heat treatment can be used to optimise their mechanical properties. Furthermore, this type of Ti alloy has a high strength at room temperature and a moderate strength at high temperature. They have higher yield strength and ultimate tensile strength when compared to α-Ti alloys. Nonetheless, (α+β)-Ti alloys have excellent corrosion resistance and a proclivity for rapid osseointegration in the human body due to the rapid formation of a TiO_2/OH film at the human-bone interface [12].

Among this class of Ti alloys, Ti−6Al−4V is first to be developed and commercialized as a biomedical Ti alloy. Although this alloy was originally developed for aerospace applications due to its exceptional properties, its high specific strength, excellent corrosion resistance, and biocompatibility have steered it toward biomedical applications. For instance, this alloy is widely recognised for its use in bone fixation and orthopaedic prostheses. A subsequent development discovered that Ti−6Al−4V contains toxic elements that cause body allergies due to the presence of vanadium (V). In order to avoid toxic release from V ions, it was replaced by Fe or Nb [13,14]. Although both of these new alloys (Ti−6Al−7Nb and Ti−5Al−2.5Fe) successfully eliminate toxic vanadium ions from Ti−6Al−4V, and even provide better wear resistance than Ti−6Al−4V, the presence of Al may cause severe health problems such as the occurrence of senile dementia of Alzheimer type diseases. Additionally, as shown in Table 1, the elastic moduli of titanium and its alloys are noticeably

Table 1 Comparison of mechanical properties between human bones with various types of titanium alloys

Material		σ_{Yield}/MPa	σ_{UTS}/MPa	E/GPa	Refs.
Cancellous bone		−	0.9−8.80	0.01−1.57	[15−17]
Cortical bone		30−70	194−195	5−23	[15]
α microstructure	cp-Ti (grade 1)	170	240	115	[18]
	cp-Ti (grade 2)	275	344	105	[19]
	cp-Ti (grade 3)	380	450	115	[18]
	cp-Ti (grade 4)	480	550	105	[1,12]
α+β microstructure	Ti−6Al−4V (annealed)	825−869	895−930	110−114	[16,20]
	Ti−6Al−7Nb	921	1024	105	[18,20]
	Ti−5Al−2.5Fe	914	1033	110	[18]
	Ti−3Al−2.5V	585	690	100	[20]
β microstructure	Ti−(10−80)Nb	760−930	900−1030	65−93	[20]
	Ti−16Nb−10Hf	730−740	850	81	[1,20]
	Ti−13Nb−13Zr	900	1030	79	[18]
	Ti−24Nb−0.5O	665	810	54	[1]
	Ti−24Nb−0.5N	665	665	43	[1]
	Ti−23Nb−0.7Ta−2Zr	280	400	55	[1]
	Ti−23Nb−0.7Ta−2Zr−1.2O	830	880	60	[1]
	Ti−35Nb−5Ta−7Zr	530	590	55	[18]
	TI−36Nb−2Ta−3Zr−0.3O	670−1150	835−1180	32	[1]
	Ti−29Nb−13Ta−4.6Zr	368	593	65	[19]
	Ti−15Mo (annealed)	544	874	78	[1,16]
	Ti−15Mo−2.8Nb−3Al	771	812	82	[18,19]
	Ti−15Mo−5Zr−3Al	870−968	882−975	75	[18]
	Ti−12Mo−6Zr−2Fe	1000−1060	1060−1100	74−85	[18,19]

greater than those of human bone. This significant mismatch in elastic moduli may contribute to implant loosening and bone resorption. When comparing Ti alloy types, both α- and (α+β)-Ti alloys have higher elastic modulus, whereas β-Ti alloys always have the lowest elastic modulus. Therefore, it is suggested that (α+β)-Ti alloys are not the best choice for biomedical implants. These factors have become a major driving force in the recently developed various compositions of β-Ti alloys.

2.3 Near-β or β-Ti alloys

β-Ti alloys consist of β-phase with the addition of β-stabilizers, whereas the near-β alloys are highly containing β-stabilizers, with some traces of α-stabilizers, but still behave as conventional β-alloys. This type of Ti alloys are readily heat treatable. As compared to Ti alloys with α-phase and mixed α+β-phases, β-Ti alloys possess lower elastic moduli, higher hardenability, and improvable ductility and toughness as they can be heat treatable [1,21,22]. The most appealing property of β-Ti alloys is their low elastic moduli, which can be used to reduce the stress shielding effect. When β-Ti is compared to near β-Ti alloys, near β-Ti alloys always have higher elastic moduli than β-Ti due to the presence of fewer α-stabilizers. Ti alloys, on the other hand, have comparable strength and biocompatibility, as well as excellent corrosion resistance in the human body environment. As a result, β-Ti alloys are currently being researched for potential use in biomedical implants.

Furthermore, β-stabilizers are divided into two types: (1) β-isomorphous elements (such as Mo, V, Ta, and Nb), and (2) β-eutectoid elements (such as Fe, Mn, Cr, Co, Ni, Cu, Si, and H) (see Fig. 4). Adding β-isomorphous elements to the formulation of Ti-based alloys always results in the formation of only one phase due to complete mutual solubility with β-Ti (Fig. 4(a)). However, due to their limited solubility in β-Ti and the formation of intermetallic compounds via eutectoid decomposition, adding β-eutectoid elements into the formulation of Ti-based alloys always results in more than one phase (Fig. 4(b)). Based on this reasoning, it is concluded that β-isomorphous elements (Mo, V, Nb, and Ta) are more desirable for use in biomedical implants because they produce only a single phase with the desired properties (such as lower elastic moduli).

3 Fabrication of Ti alloys

In the fabrication of Ti-based alloys, there are conventional methods (such as powder metallurgy and casting) and advanced methods (such as selective laser melting and electron beam melting) [23−25]. This review focuses on the most common processing routes ever used to produce Ti-based alloys, which are powder metallurgy with multiple sintering routes and additive manufacturing routes, as discovered through a literature search.

3.1 Powder metallurgy

Over the decades, there has always been a global demand for a low-cost manufacturing process for producing high-performance Ti alloys. Powder metallurgy (PM) is undeniably a promising candidate for low-cost-high-performance manufacturing processes [26].

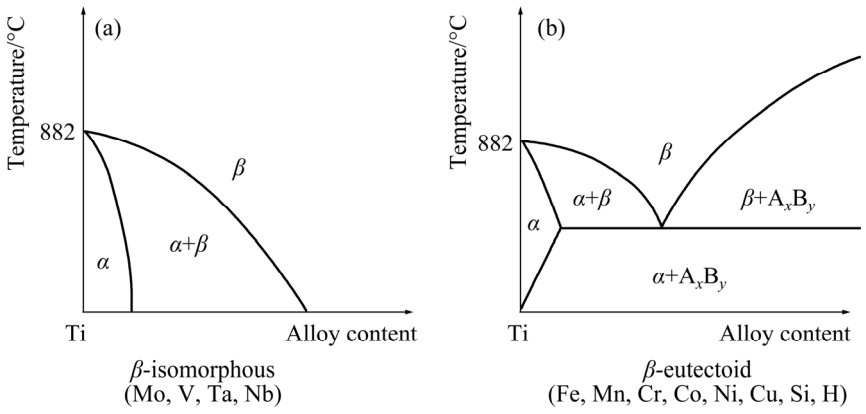

Fig. 4 β-stabilizing element effect of β-isomorphous elements on Ti (a), and effect of β-eutectoid elements on Ti (b) (Reprinted with permission from Ref. [10]. Copyright 2013, Elsevier)

Powder metallurgy is a method of consolidation for fine metal particles into usable engineering components such as aerospace components and cryogenic devices. For many years, it has been well-established in the industrial field and has involved various types of materials such as iron (Fe) and copper (Cu). Figure 5 depicts the basic working principle of powder metallurgy. The precursor, which is typically in the form of elemental metallic powders along with the alloying elements, must go through a mixing or mechanical alloying process to induce alloying between the metal powders, or, in some cases, the powders are already pre-alloyed by atomization process. Consolidation of the alloyed metal powders is accomplished through pressing at an optimum pressure and subsequent sintering near full density. This series of steps allow the densities of the product to approach 100% while also increasing the bonding between particles to achieve densification for the finished products [27].

Sintering is a critical process in the powder metallurgy process flow because it determines the final properties of the resultant alloy. Sintering is a process that uses heat energy to consolidate powder compacts into sintered products. Densification, grain growth, and microstructure evolution are the fundamental processes that occur during sintering. During sintering, the pores between the powder particles gradually shrink as the sintering process progresses, a process known as necking. Reduced pores and lower interfacial energy between grain boundaries always benefit densification and provide precise control over grain size, sintered density, and phase distribution in the alloy [28]. The sections that follow provide a brief overview of various sintering routes in the powder metallurgy process, such as pressure-assisted sintering (spark plasma sintering) and pressure less sintering (microwave sintering).

3.1.1 Spark plasma sintering

Spark plasma sintering (SPS) is a new technique, where a pulsed electric field (DC current) is combined with the high temperature to assist the densification of a powder metallurgy product. The SPS is also known as pulsed electric current sintering (PECS) and the technique is undeniably time-saving, due to removing the need for powder consolidation through normal cold pressing and a shorter duration of sintering time. The sintering process in the conventional press-and-sinter method takes several hours; however, in SPS, the densification process is very fast, taking only a few minutes and often at lower temperatures [28]. Furthermore, one of the elitisms of SPS is the ability to fabricate high-performance bulk alloys with much finer grains than those fabricated through conventional hot pressing and hot isostatic pressing [29].

The precursor alloy powders are an important consideration when fabricating Ti alloys using the spark plasma sintering route. Numerous studies have indicated that densification of alloy powders would be enhanced if they were milled or mechanically alloyed rather than gas atomized. Densification rates for milled powders are reported to be higher than those for atomized powders, owing to their respective powder morphologies. When the particle size is small, the irregular shape of milled powders always has a higher surface energy. Increased surface energy associated with irregular geometry in milled powders has historically been beneficial in accelerating powder shrinkage and densification [30−32]. Additionally, sintering parameters such as those listed in Table 2 for various Ti alloys must be carefully considered, as they have a significant impact on electrical, mass, and thermal transport during sintering.

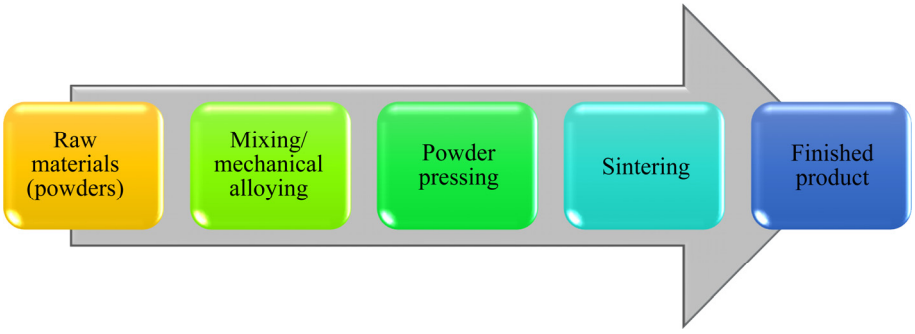

Fig. 5 Powder metallurgy (PM) process flow

Table 2 Various Ti alloy systems fabricated via spark plasma sintering method

Material	Sintering parameter			Resultant property			Ref.
	Temperature/ °C	Pressure/ MPa	Time/ min	Phase present	Ultimate strength/MPa	Elastic modulus/GPa	
Ti−*x*Nb (*x*=30−47)	900−1300	50	60	Homogeneous β	Not reported	80−90	[33]
Ti−13Nb−13Zr	700−900	30	10	β with some amount of α and α''	830−1790	Not reported	[34]
Ti−20Nb−13Zr (at.%)	800−1200	50	10	$\alpha+\beta$	Not reported	Not reported	[35]
Ti−(30−35)Nb−(5−20)Ta −(5−7)Zr	1100	50	5	β	Not reported	66−149	[21]
Ti−35Nb−7Zr−*x*Cu (*x*=4, 7, 10, 13)	1000	40	5	β	1374−1856	57−79	[22]
Ti−35Nb−7Zr−5Ta	800−1100	50	5−20	$\alpha+\beta$	1350−2120	72−94	[36]
$Ti_{65.5}Nb_{22.3}Zr_{4.6}Ta_{1.6}Fe_6$ (at.%)	960	3	5−30	β+FeTi	2530−2650	72−75	[37]
$(Ti_{69.7}Nb_{23.7}Zr_{4.9}Ta_{1.7})_{100-x}Si_x$ (*x*=0, 2, 5) (at.%)	960	50	5	β+$(Ti, Zr)_2Si$	2793−3267	35−40	[38]
Ti−5Mo−5Ag	800−900	60	Not reported	β	1941−2100	Not reported	[39]
Ti−*x*Mo (*x*=4−20)	1200	50	5	β	440−800	111−127	[40]
Ti−5Al−2.5Fe	750−850	5	5	Not reported	250−300	Not reported	[41]

It is observed that when fabricating biomedical-grade Ti alloys that always contain Nb, Zr, and Ta as the beneficial β-stabilizer, spark plasma sintering is always a viable option. The combination of metallic elements such as Ti, Nb, Zr and Ta is actually quite difficult to be melted homogeneously through the traditional melt-and- cast solidification, due to large differences in the melting point and specific gravity. High heating rate up to ~727 °C/min and short sintering time of several minutes offered in spark plasma sintering are very beneficial to preparing some new materials with finer grains and varieties in the precipitated phase [36,37].

3.1.2 Microwave sintering

There is also a pressureless sintering route, in addition to pressure assisted sintering routes such as spark plasma sintering (SPS), hot pressing (HP), and hot isostatic pressing (HIP). This route sinters the alloys without the use of pressure, which is typically done in a microwave, vacuum, or a controlled inert atmosphere at the atmospheric pressure [42]. The fabrication method still requires the precursor powder to be uniaxially pressed under optimum pressure, yielding green compacts, before sintering in a furnace under a high purity inert atmosphere. According to a literature search, the microwave sintering (MW) route has been extensively investigated due to the effectiveness of its heat transfer mechanism, which is capable of shortening the sintering cycle of Ti alloys, thereby limiting grain growth and lowering manufacturing costs [43]. However, similar to vacuum sintering, these two types of pressureless sintering processes do not allow for full densification of Ti alloys and frequently left porosity in the sintered microstructure [43]. When spark plasma sintering (SPS) is compared to microwave sintering (MW), it is discovered that alloys sintered via SPS have a reduced porosity, whereas those sintered via MW sintering have a much more porous structure, which actually aids in lowering the elastic modulus of Ti alloys designed for implant application [44]. Furthermore, the presence of pores in Ti alloys improves osseointegration, which refers to the formation of a bond between the living bone and the surface of the implant materials [45]. It is still unclear what the relationship between pore size and

the osseointegration process is. However, a wide range of pore sizes between 400 and 700 μm, and even up to 1.2 mm, has been reported to show sufficient evidence of bone cell growth following implantation. Aside from that, most scientific studies believe that the optimal pore sizes for bone healing are in the range of 150−600 μm. Higher porosity was expected to promote bone healing in this regard; however, it is also important to carefully control the pore size and porosity, as higher porosity will cause the mechanical properties of the implant material to be reduced [46].

Fundamentally, in MW sintering, the heating process occurs at the core or centre of the samples as the materials absorb microwave radiation and convert it into heat energy, which is then distributed throughout the samples. This heat transfer occurs from the sample's core to the entire samples volumetrically (direction of heating is from inside to outside). However, this phenomenon contradicts the conventional heating process, in which heat is initially transferred to the surface and then transferred to the entire sample via conduction, convection, and radiation (direction of heating is from outside to inside). In short, variation in temperature gradients of different areas of the samples in conventional heating results in poorer microstructure and mechanical performance than in microwave sintering [47]. Table 3 lists some Ti alloys and composite systems that have been developed via microwave sintering route and have a significant insight on the porous structure with a reduction in their elastic modulus.

3.1.3 Conventional press-and-sinter

In the powder metallurgy process, the conventional press-and-sinter method usually requires the alloys to be synthesized through mechanical alloying methods, though pre-alloyed powders are also commonly used. The alloy powders are then cold pressed to form green compacts, which are sintered in a conventional tube furnace under specific conditions. Controlling the processing parameters is critical in order to produce Ti alloy with desired properties. The milling speed and milling time remain the most important parameters to control during the mechanical alloying process. According to a search of the literature on mechanical alloying processes for Ti alloys and composites fabrication, the milling speed is typically 200−300 r/min, with milling time ranging from 2 to 40 h [53,54]. The important process that occurs during mechanical alloying in high energy ball milling is the countless repetition of fracturing and cold welding phenomena between the powder particles to impart the alloying process homogeneously while simultaneously refining the particle size [55,56]. High energy ball milling frequently produces powder with smaller particle size, with proper sintering control, and leads to refinement of the grain size, which benefits mechanical performance [57].

Following the synthesis of alloy powders, the powders must be consolidated into green compacts by cold pressing. This process applies optimum pressure to the compact, allowing it to achieve sufficient green strength prior to sintering. Several studies on the fabrication of Ti-based alloys via powder metallurgy reported a wide range of compaction pressure, ranging from 150 to 690 MPa. However, green density has been reported to be at its optimum state when compaction pressure is between 500 and 550 MPa [24,58−60]. Following

Table 3 Various Ti-based alloys and composites fabricated through route of microwave sintering

Material	Sintering temperature/°C	Dwell time/min	Heating rate/(°C·min^{-1})	Pore size or percentage of porosity	Elastic modulus/GPa	Ref.
cp−Ti Ti−6Al−4V Ti−5Fe	1200−1400	3−30	31	>5 μm	N/A	[43]
Ti−23Nb (at.%)	900−1200	10−30	30	9.8−24 μm	6.6−9.2	[45]
Ti−*x*Mo (*x*=5−20 wt.%)	1050	20	20−30	34%−42%	2.5−9.1	[48]
Ti−3Cu	650−800	20	10	24.6 %	7.0−11.9	[49]
Ti6Al4V/HA	950−1100	30	N/A	11.3%−12.1%	15.1−39.2	[50]
Ti−Nb/*x*HA (*x*=0−20 wt.%)	1500	5	N/A	150−260 μm	12.5−29	[51]
Ti−30Nb/20HA	1500	5	N/A	20−30 μm	20	[52]

the compaction of green bodies, sintering is carried out at high temperatures, which are typically 70%−85% of the melting temperatures of the host elements that comprise the alloys, which are approximately 1100−1400 °C for Ti-based alloys [59,61].

To summarize, the PM method is widely used because of its primary driving force: cost and material savings. It also offers a number of advantages on finished products, such as products with near-net-shape (NNS), comparable mechanical properties, fully dense or porous structure, and nearly homogeneous microstructure. The disadvantages of PM methods are high raw material and tooling costs (mould for compaction) and difficulties in producing parts with intricate shapes. The PM process has long been recognized as a good choice for fabricating Ti-based alloys and is still used in mass production today.

Conventional fabrication methods, such as powder metallurgy, have been developed over decades. Even though conventional methods have limitations (such as slow production rate, difficulty in parameter control, and geometry shape limit), the consistency and stability of producing a homogeneous alloy and composites is high. This is why traditional methods are still used in industries.

3.2 Advanced fabrication methods

Advanced fabrication methods, also known as additive manufacturing (AM), are a new technology that offers improved performance for Ti-based alloys and composites used in implant materials. When compared to the conventional fabrication methods, additive manufacturing is more pronounced in producing porous structures, which are said to closely resemble the characteristics of bone. According to current knowledge, additive manufacturing methods are divided into two systems: powder-bed fusion and powder-fed fusion. Figure 6 depicts the classification of well-known additive manufacturing routes. This sub-section would provide an in-depth examination of several recently developed additive manufacturing processes.

3.2.1 Selective laser melting

Selective laser melting (SLM) is one of the most widely used additive manufacturing (AM) techniques which has gained popularity in recent years. This method is very useful in manufacturing three-dimensional structures with intricate designs by using a high-power laser source to melt the starting raw material powder while layer-by-layer stacking [61,62]. SLM requires a laser beam with a computer-controlled process to create 3D-parts on a powder bed, according to the system's Computer Aided Designed (CAD) model. The primary principle of SLM is the melting of metal powders using a laser beam to create a liquid pool, which is rapidly solidified on the powder bed directly adjacent to the laser-scanning-spot. Once a layer of the model is completely solidified, the building plate moves down to complete the melting-and-solidification process of the raw powders layer-by-layer, consolidating the material together and forming final products [23]. Figure 7 shows a schematic diagram of selective laser melting (SLM). The mechanism of the SLM process is nearly identical to that of electron beam melting (EBM), with the main difference being the source used to melt the powder, which can be either a laser source in SLM or an electron source in electron beam melting (EBM). SLM has been reported to be capable of fabricating complex part designs with improved accuracy and finer structure when compared to other 3D printing technologies such as EBM and laser engineering near net shape (LENS) [61].

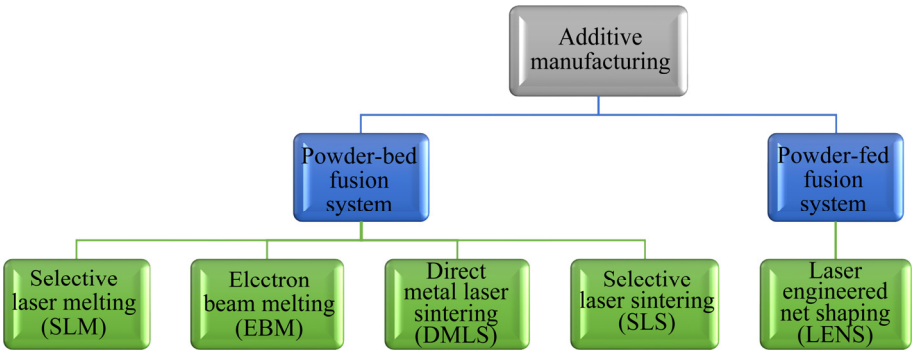

Fig. 6 Classification of additive manufacturing processes

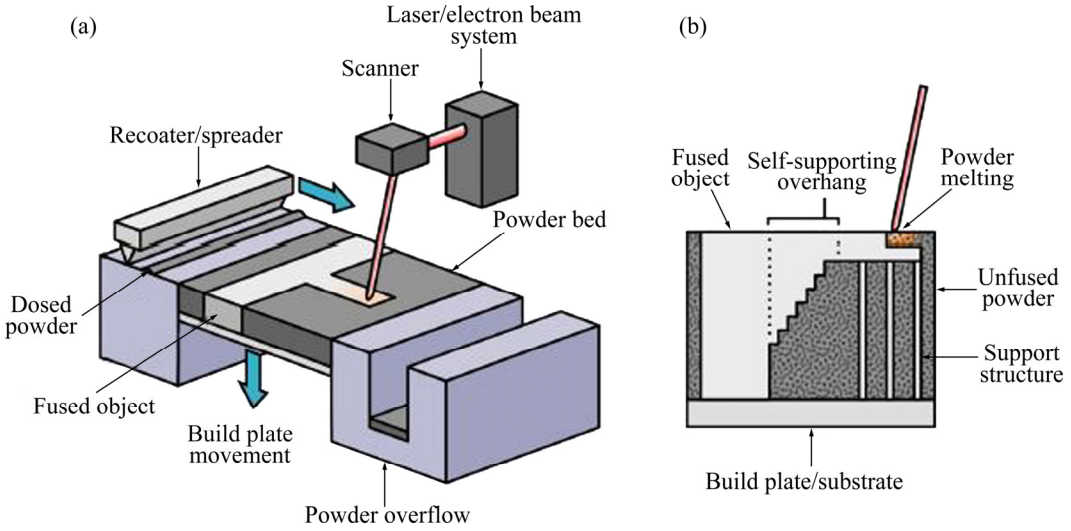

Fig. 7 Schematic diagram illustrating process of selective laser melting (SLM): (a) Common physical layout of equipment (Dosed powder is distributed on the substrate and powder bed melts upon heats from the laser source. The build plate moves downwards, another layer of powder is distributed, the powder melts upon heating and rapidly solidified, layer-by-layer until final product is completed); (b) Cross section of building plate (Reprinted with permission from Ref. [62], Copyright 2019, Elsevier)

In general, SLM technology is used on highly complex geometry components that are nearly impossible to fabricate using conventional manufacturing methods (e.g. casting and powder metallurgy). The remnant porosity or defects that occur in the fabricated parts as a result of layer-by-layer stacking, overlapping of the melt pools, temperature gradient in the build-ups layer, and rapid solidification produced by a fast-moving laser source are major concerns with this process. These issues must be addressed by paying close attention to critical SLM process parameters such as scan speed, hatch spacing, laser power, and powder layer thickness. These parameters have a significant impact on the inner porosity structure and, as a result, the mechanical properties [63]. Table 4 combines some important parameters of selective laser melting for biocompatible Ti-based materials, as well as their important mechanical properties.

Due to the general high heating and cooling rates, SLM fabricated parts always have fine microstructures, whereas the mechanism of layer-by-layer stacking generates anisotropic and heterogeneity mechanical response. This type of behaviour is highly dependent on the process parameters, as shown in Table 4. The elitism of the SLM process over conventional processing routes provides numerous advantages, including shorter production time, almost no geometric restriction with a highly automated process, and better mechanical compatibility with human physiological needs. Furthermore, the SLM process's unique ability to produce complex geometries products such as honeycomb type structures (porous structure) aids bone cell growth because the porous structure resembles human trabecular bone. Some of the challenges encountered include the loss of superelastic behaviour as compared to conventionally manufactured parts, precise control over processing parameters, a pre-process for feedstock (Ti alloy powder) is required (such as atomization), a post-process finish is required (such as cutting edges), expensive tooling, and shielding gas [69,78,81].

3.2.2 Electron beam melting (EBM)

Electron beam melting (EBM) is another technique that is currently researched as part of the broad range of additive manufacturing processes. The process, like SLM, used 3-dimensional printing, except that EBM used electron beam energy to melt the metal powder. The EBM system employs an electron gun with a high power of 60 kW to generate a focused electron beam with an energy density greater than 100 kW/cm^2. Electromagnetic lenses control the focus of the electron beam, while deflection coils control the movement of the beam on the building table. During the building process of a part, powder with a thickness of 0.1 mm is

Table 4 Processing parameter of selective laser melting of Ti and its alloys

Material	Parameter				Resultant properties				Ref.
	Laser power/ W	Scanning speed/ (mm·s^{-1})	Scanning spacing/ mm	Powder layer thickness/ mm	Phase present	Porosity/ %	Elastic modulus/ GPa	Ultimate strength/ MPa	
cp-Ti	122−166	400	0.12	0.03	α-Ti	99% fully dense	105.4−114.7	714−1014	[64]
cp-Ti	120−440	1000	0.12	0.03	α-Ti	N/A	N/A	408.8−509.0	[65]
cp-Ti (grade 1)	100	385	0.12	0.03	α-Ti	(68−73)%	1.47−2.68	59.4−75.0	[66]
cp-Ti (grade Ti), Ti−6Al−4V	200	1000	0.10	0.05	α-Ti (cp−Ti), α+α'−Ti (Ti−6Al−4V)	72%	N/A	658 (cp-Ti), 1170 (Ti−6Al−4V)	[67]
Ti−xNb alloys (x=25−61 wt.%)	330	1000	0.10	0.03	β-Ti	97% fully dense	18.7−24.5	751−1030	[68]
Ti−50Ta alloys	120−360	400−1200	0.125	0.05	β-Ti	99.85% fully dense	N/A	N/A	[69]
Ti−xTa alloys (x=0−25 wt.%)	220−380	600−1400	0.07	0.05	α'+β	<95% fully dense	89−115	641−1186	[70]
Ti−15Ta−xZr (x=1.5−15.5)	350−400	205	0.115	25	α+β	N/A	42.9−92.18	698.91−960.29	[71]
Ti−35Zr−28Nb	100−180	347−1250	0.12	0.03	β	2.0% (bulk), 49.9% (porous)	57.0−60.2 (bulk), 1.0−1.3 (porous)	45−58 (porous)	[72]
Ti−6Al−4V	90	600	0.08	0.03	Martensite α'-Ti	99.74% fully dense	N/A	N/A	[73]
Ti−6Al−4V	180	1350	0.1	0.03	α+β	(48.83−74.28)%	1.93−5.24	44.9−237.5	[74]
Ti−6Al−4V−5Cu	200	1000	0.12	0.05	α+β	98.5% fully dense	110	1600	[75]
Ti−6Al−4V−0.5Ag	200	1000	0.12	0.05	Martensite α'-Ti	98.7% fully dense	113.5	1180	[75]
Ti−30Nb−5Ta−3Zr	200	N/A	0.05−0.075	0.05	β-Ti	77.23%	64.2	680	[76]
Ti−Nb−Zr−Ta−Si	250	1400	0.06	0.03	β-Ti	N/A	59.2−71.3	538−1120	[77]
Ti−6Al−2Zr−1Mo−1V	180−380	300−800	0.12	0.03−0.06	Martensite α'-Ti	99.36% fully dense	N/A	780.6−1422.1	[78]
Ti−25Nb−3Zr−3Mo−2Sn	300	1000	N/A	0.05	β-Ti	N/A	N/A	716	[79]
Ti/nano-HA	240	1000	0.08	0.03	α, Ti_5P_3, $CaTiO_3$	N/A	28.86	289.01	[80]

spread over the building table from two hoppers inside the build chamber. Before preheating and melting process by the electron beam, the powder from both sides is fetched by a moving rake and spread across the table [82].

It is critical to note that temperature

differences in the powder bed during the building process of a part frequently result in variations in phase and microstructure formation. According to Table 5, the high temperature of the powder bed and relatively slow cooling rate in the EBM process frequently causes the alloy to form the α+β phase, which tends to increase the Young's modulus of the alloy, which is often avoided when synthesizing alloy targeted for implant application. In contrast to EBM, SLM-produced parts always have a desirable β-Ti microstructure due to the lower temperature of the powder bed (~200 °C), which leads to a reduction in Young's modulus [83]. Since the build process in EBM typically takes up to 10 h, it is similar to the aging process, which is frequently carried out at a temperature of 400−500 °C for 10 h, which is becoming a contributing factor in suppressing the formation of single β-phase [84]. Table 5 examines key differences between biocompatible Ti-alloys fabricated using SLM and EBM.

In conclusion, the titanium-based alloy processing methods are as follows.

(1) Cost effectiveness

In terms of cost, the conventional route, such as powder metallurgy, uses a lower cost to achieve the fundamental requirements for an implant, such as mechanical properties and biocompatibility. Implementation of additive manufacturing methods such as SLM, EBM, and any other methods classified as additive manufacturing always necessitates a higher cost in terms of equipment setup and raw material utilization efficiency.

(2) Dimensional accuracy and intricacy

In real biomedical applications, the dimension of an implant is absolutely critical to human bone, and the implant is frequently custom made prior to the implantation process. In terms of dimensional accuracy and intricacy, additive manufacturing techniques such as SLM and EBM are always the best choices for producing implants with high precision dimensions and intricate shapes.

(3) Pore-size control

Additive manufacturing has the advantage of pore size control because the process has the capability of customizing the parts whether they are built with a highly dense or highly porous structure. As for the conventional route, such as powder metallurgy, the process is also capable of fabricating porous structures through the use of space holders in the fabrication process; however, controlling the pore size as sintering proceeds would be quite challenging. Additionally, an appropriate porous structure design would then aid in enhancing bone-to-implant osseointegration following implantation to injured parts. As a result, pore-size control should be a priority, as it is relatively easy to control in SLM/EBM processing but quite hard to control properly in PM fabrication.

(4) Homogeneity in microstructure

When compared to conventional methods, additive manufacturing has always been reported to have heterogeneity and anisotropic properties in microstructure and mechanical performance. Due to the obvious repeated process of melting and solidifying that occurs layer by layer in any additive manufacturing process, obtaining a homogeneous microstructure is quite difficult.

A good fabrication method for Ti alloys, on the other hand, should provide the required properties for the application. The desired phase (β-phase) that always comes with lower elastic modulus, homogeneity in microstructure, good mechanical strength, proper pores formation, and bioactivity are some of the main characteristics for a Ti alloy to be medically qualified as a biomedical implant. Prior to alloy fabrication, process selection is critical because different processes result in different final alloy properties.

Table 5 Comparison of process parameters and properties of Ti−24Nb−4Zr−8Sn alloy fabricated through EBM and SLM

Method	Porous/ dense	Scanning speed/ ($mm \cdot s^{-1}$)	Electron/laser spot size/μm	Layer thickness/ μm	Initial temperature/ °C	Phase present	Ultimate strength/ MPa	Elastic modulus/ GPa	Ref.
EBM	75% porous	150	200	70	500	(α+β)-Ti	45	1.34	[83]
EBM	70% porous	150−900	N/A	70	500	(α+β)-Ti	35	0.7	[84]
SLM	75% porous	750	40	50	200	β-Ti	50	0.95	[83]
SLM	Dense	50−900	80	100	N/A	β-Ti	665	53	[85]

4 Properties of Ti alloys

The properties of a substance are critical in determining its application. This section is divided into two topics that are bulk properties and surface oxide properties on Ti alloys, in order to determine the properties of Ti alloys that are ideal for commercialization as a biomedical implant.

4.1 Bulk properties

4.1.1 Young's modulus/elastic modulus

There are two major issues with Ti-based alloys that have been commercialized as bone implant materials: commercially pure Ti (cp-Ti) and Ti−6Al−4V alloys. The key issues raised by orthopaedic practitioners are stress shielding due to the large difference between the implant materials and the adjacent bone, and long-term health issues caused by the harmful ions released by the implant materials, such as neurodegenerative disease (Alzheimer's and dementia) [67,86,87]. The Young's modulus, which is similar to human bone, is the primary requirement for implant material to be considered. A large mismatch in Young's modulus between adjacent bone and implant material, resulting in a stress shielding effect, is always the cause of bone resorption, bone fracture, or unexpected implant failure. The mismatch frequently causes excessive movement between the implant and the bone, preventing stress from being transferred from the implant to the neighbouring bone. The implant will then loosen, inhibiting new bone growth and isolating the implant from the implantation site [16,81].

Currently, the elastic moduli of implant materials employed are stainless steels (200 GPa), Co−Cr alloys (240 GPa) and Ti-based alloys (105−125 GPa) [20,88]. In general, the elastic modulus of human cortical bone is approximately (17±1) GPa, or can be stated in the range of 10−30 GPa [65,89]. As a result, Ti-alloys carefully designed to have β-phase are thought to be suitable for use as implants due to their low elastic modulus of 50−80 GPa, which is still two or three folds that of human bone's modulus [90]. The key factor that determining the phases present in any Ti-based alloys is the alloying element and how it is behaving to modify the crystal structure of Ti, whether it is hexagonal close-packed which leads to the formation of α-phase or body centered-cubic crystal structure that always leads to the formation of β-phase. When producing Ti-based alloys with low modulus, a higher amount of β-phase is always beneficial in lowering the high modulus of the metals [88]. Table 6 lists the most commonly reported low modulus Ti-alloys synthesized with various β-stabilizers (β-isomorphous: V, Mo, Nb, Ta, Re, and β-eutectoid: Fe, Mn, Cr) and their elastic modulus. From Table 6, it can be seen that, despite the fact that a lot of alloying elements are being added to the titanium system for the primary purpose of changing the α-phase to become β-phase and subsequently lowering the elastic modulus, the elastic modulus values of the alloys are still not approaching that of human bones. As a consequence, much research remains to be done in order to fabricate Ti-based implants that can closely mimic the elastic modulus of bone.

4.1.2 Biocompatibility

Biocompatibility is generally defined as the ability of a foreign material to be accepted in the human body environment without causing any undesirable effects such as inflammatory or allergic reactions. The degree of biocompatibility of a material is directly related to the cytotoxicity, possibility of toxic-ions release, and corrosion behaviour of the material when evaluating biocompatibility [109]. The assessment of biocompatibility encompasses a wide range of topics, including cytotoxicity (evaluation of biomaterials for being toxic and killing cells), hemocompatibility (evaluation of the materials for the possibility of causing adverse effects on red blood cells and the blood circulation system), carcinogenicity (investigation to determine whether the materials would be a source of inducing cancerous cells), genotoxicity, irritation, and inflammation [20,110]. Figure 8 summarises four types of body responses to foreign material implantation. According to the figure, Ti is widely recognized as a nearly inert biomaterial owing to its superior corrosion resistance due to the spontaneous formation of a passive oxide layer on its native surface. Due to the absence or very long time required to form the bonding between adjacent bone and implant, the healing time for a patient will be very long due to nearly inert property of Ti. This bonding is known as osseointegration, and it is

Table 6 Ti-based alloy with addition of various β-stabilizers

Alloy composition/wt.%	Processing	Alloy type	Elastic modulus/GPa	Ref.
Ti−5Nb	Casting+AT	$\alpha+\beta$	127	[91]
Ti−10Nb	Casting+AT	$\alpha+\beta$	149	[91]
Ti−15Nb	Casting+AT	$\alpha+\beta$	114	[91]
Ti−20Nb	Casting+AT	$\alpha+\beta$	127	[91]
Ti−20Nb	Casting+annealing+HF+AT	α''	110	[92]
Ti−28Nb	As-cast	$\alpha''+\beta$	81	[93]
Ti−33Nb	PM	β	107	[94]
Ti−30Nb	Casting+ST+CR	β	45−67	[95]
Ti−40Nb	Casting+annealing+HF+AT	β	76−88	[92]
Ti−40Nb	PM	β	76	[94]
Ti−40Nb	Casting+ST+CR	β	45−67	[95]
Ti−40Nb	PM	β	65.10	[96]
Ti−45Nb	Casting+HR+ST	β	64.3	[97]
Ti−56Nb	PM	β	59	[94]
Ti−50Ta	Casting+CR+ST+AT	α''	77−88	[98]
Ti−10Mo (porous)	Selective laser sintering	$\alpha+\beta$	10−20	[99]
Ti−xMo (x=15−18)	Casting+HR+ST+CR	$\beta+\omega$	73−84	[100]
Ti−xCr (x=10−14)	Casting+HR+ST+CR	β-Ti	68−82	[101]
Ti−Fe−xNb (x=0−11)	As-cast	100% β-Ti (11 wt.% Nb)	84−129	[102]
Ti−8Fe−8Ta	Casting+CR+ST+AT	β	N/A	[103]
Ti−xFe−yTa (x=8−10, y=0−10)	As-cast	$\alpha''+\beta$	92.56−107.33	[104]
Ti−10Zr−xMo (x=1−20)	As-cast	β-Ti (Mo>7.5 wt.%)	87−96 (bending)	[105]
Ti−25Nb−(1−5)Sn−(2−4)Cr	As-cast	β-Ti	66−78	[106]
Ti−Nb−Zr−Mo	As-cast	β-Ti	68−73	[107]
Ti−35Nb−4Sn−6Mo−xZr (x=0−15)	Casting+HF+ST	β-Ti	68−92	[108]

ST: Solution treatment; HR/CR: Hot/cold rolling; HF: Hot forging; AT: Aging treatment; PM: Powder metallurgy

extremely helpful in initiating the healing process. Aside from the goal of lowering the modulus, osseointegration issue is a key indicator of biocompatibility.

Figure 9 depicts the alloying elements that have been identified as no longer biocompatible for use in implant materials. From Table 6, the most common alloying elements added to Ti are Nb, Ta, Mo, and Zr, which have lower toxicity and better biocompatibility than V and Al, which have long been used as alloying elements in the formulation of Ti−6Al−4V. Ti−6Al−4V has been identified as no longer representing biocompatible characteristics after a long period of routine use as implant material, due to harmful ions released by aluminium and vanadium that caused numerous health issues [3]. According to this point of view, the most important step before synthesis of a titanium alloy is the selection of alloying elements. The alloying elements classified as beta-stabilizers have been demonstrated to be biocompatible for incorporation into Ti systems with the primary purpose of lowering the elastic modulus while posing no toxicity effect to human physiological systems upon implantation.

4.2 Surface oxide properties

4.2.1 Bioactivity

Bioactivity is an important property that should be inherited by implant materials, and it

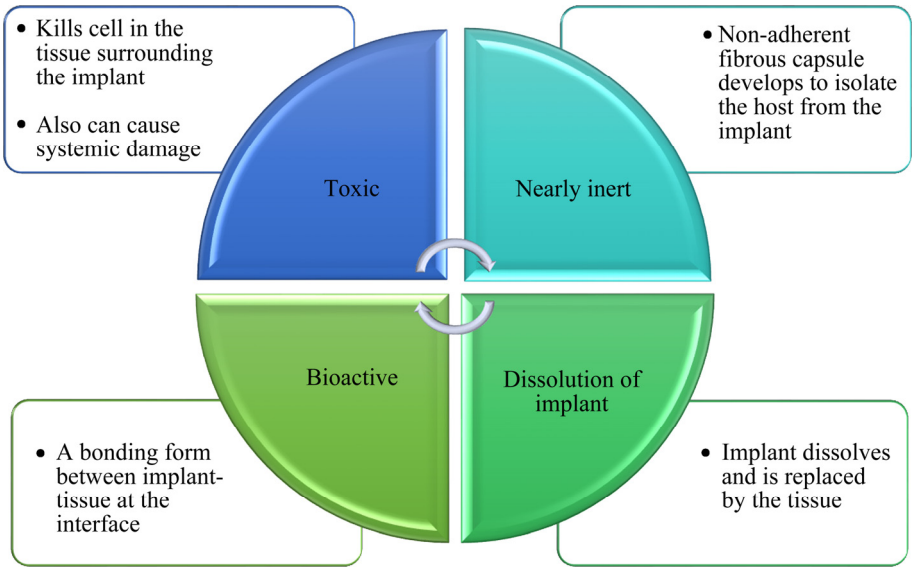

Fig. 8 Four responses of bone-to-implant materials

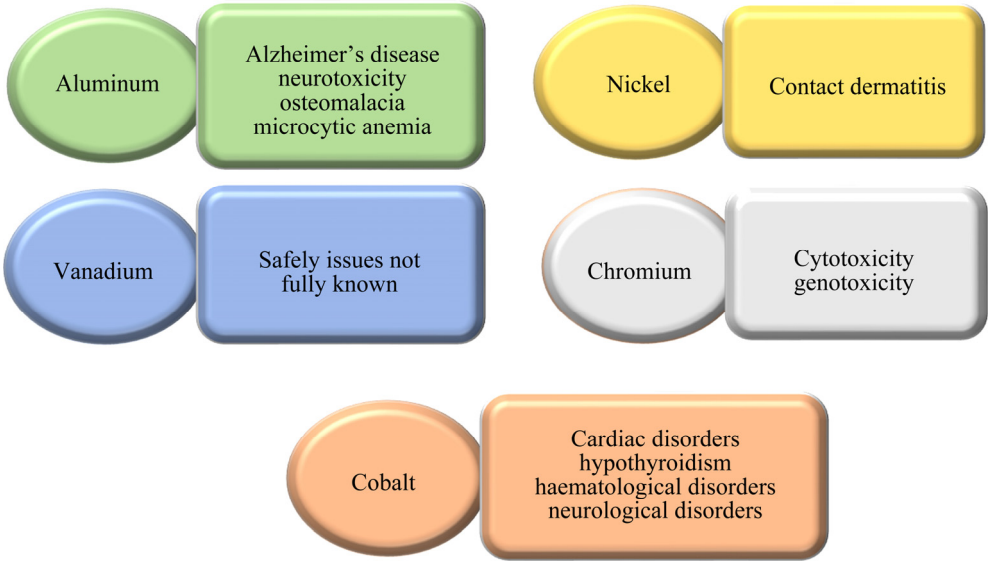

Fig. 9 Alloying elements harmful to be used in formulation of Ti based alloys

refers to a material's ability to induce specific biological activity and invigorate a response between the bone and the implant material [111]. However, in the case of a titanium-based implant, it is widely acknowledged that titanium is nearly inert, even in body environments, due to the passive oxide layer formed on its surface, which also acts as a barrier to corrosion attack. Many efforts have been focused on surface modification methods in order to produce this bioactive surface on Ti-based alloys.

4.2.2 Surface oxide topography and phase structure

A specific surface oxide layer for Ti alloy is beneficial to aiding in the process of new bone growth. One of the most important factors to consider is the phase structure. The surface modification used should result in the formation of a nano-scale surface oxide (TiO_2) layer. This is due to the fact that bone cells prefer implants with a nano-phase surface. Human bone is built up by inorganic calcium phosphate mineral such as calcium dihydrogen phosphate ($Ca(H_2PO_4)_2$), calcium hydrogen phosphate ($CaHPO_4$) and organic protein, as well as collagen, in nanostructured form [112]. This finding is consistent with several studies, demonstrating that a nano-scale regime on the metal surface creates spaces for protein absorption, thereby improving the interaction

between bone and implant [113,114]. As a result, it can be concluded that human bone cells adhered better to nano-phase regime metals than to other phases (for example: micro-phase).

Furthermore, the topography of Ti alloys with nanotubular surfaces can improve bone bonding strength, osteoblast proliferation, and ions adsorption, as well as adhesion, resulting in better performance in in-vivo studies [115]. This is due to its lateral spacing feature. The lateral spacing may increase the surface-contact area of the human bone cell, improving bone cell adhesion even further. Using this theory, numerous case studies have been reported to demonstrate the outstanding performance of the nanotubular structures established on the Ti-based alloys for the implant applications [112−114,116].

When it comes to the crystal structure of the surface oxide, annealed surface oxide nanotubes (on Ti alloy) with crystalline structure are preferred over TiO_2 nanotubes with the amorphous structure. Several case studies have clearly shown that the annealed surface oxide nanotubes (on Ti alloy) with crystalline structure promotes better apatite-growth in the human bone than those with the amorphous structure [117,118]. However, the as-grown TiO_2 nanotubes (without secondary surface treatment) mostly have amorphous structure [119]. Therefore, the annealing treatment is required to modify the crystal structure of the TiO_2 nanotubes on the surface of Ti alloy.

Several case studies on pure Ti surface oxide nanotubes (TNTs) as biomedical implants can be used to determine the appropriate annealing temperature for obtaining good bioactivity phases. The studies reported that annealing the TiO_2 nanotubes at 550 °C transforms the phase to become a mixture of anatase and rutile phase, which promotes better apatite formation than annealing the nanotubes at 450 °C with primarily anatase phase [117,120]. Furthermore, when the annealing temperature exceeds 600 °C, the nanotubular structure on Ti alloy becomes distorted and collapses [117,119]. Figure 10 depicts the changes in TiO_2 nanotube structure as the annealing temperatures were varied from 450 to 750 °C. Based on the micrographs, it can be concluded that nanotubes annealed at 450 °C are nearly identical to as-grown TiO_2 nanotubes. However, increasing the annealing temperatures to 600 and 750 °C revealed that the well-ordered arrangement of the nanotubes began to degrade, resulting in the dense rutile

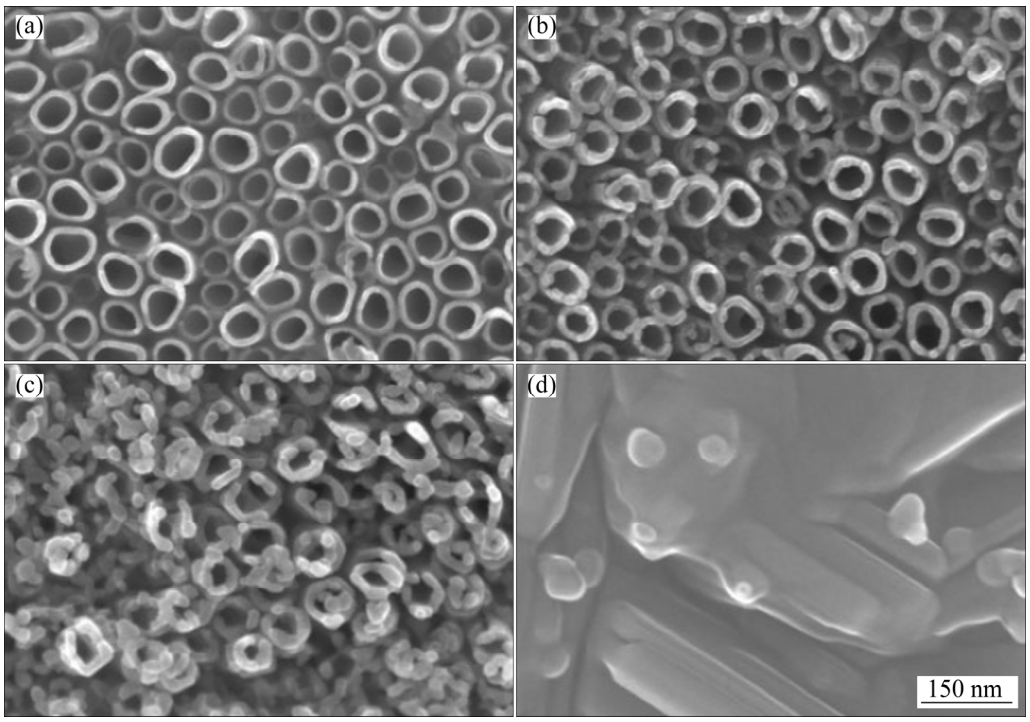

Fig. 10 FESEM micrographs of TiO_2 nanotubes: (a) As-grown nanotubes; (b) As-annealed nanotubes at 450 °C; (c) As-annealed nanotubes at 600 °C; (d) As-annealed nanotubes at 750 °C (Reprinted with permission from Ref. [117]. Copyright 2011, John Wiley and Sons)

phase [117]. Based on this observation, it is reasonable to conclude that, in order to achieve the best bioactivity of TiO_2 nanotubes grown on Ti-based implants, a mixture of anatase and rutile phase is recommended, with annealing temperatures ranging from 400 to 550 °C used to avoid structure rupture.

4.2.3 Surface roughness

In general, as the roughness of a surface oxide layer increases, so does the osseointegration of the orthopaedic implant. Despite the fact that there is no standard for the specific surface roughness that must be established on the surface of an implant, a scientific finding claims that moderately rough surfaces improve osteoblast proliferation and collagen synthesis [121]. The surface roughness is estimated to be around 68 nm because the most commonly used implant, Ti−6Al−4V with surface oxide nanotubes, has an average surface roughness of (R_a=(68±7) nm) [122]. The nanotubular structure is an excellent choice for improving surface roughness as an implant. The inter-tubular spacing (or pore diameter) within the surface oxide nanotubes of Ti alloy is the most important factor affecting surface roughness [123].

According to Table 7, increasing the annealing temperature from 450 to 600 °C increased the diameter of Ti−7.5Mo surface oxide. Surface roughness was significantly reduced when diameter values of 60 and 80 nm were assumed to be equivalent to inter-tubular spacing (by ignoring tube wall thickness). Finally, higher surface roughness produced more apatite than lower surface roughness.

In summary, a moderate surface roughness (approximately 68 nm) of surface oxide on Ti alloy improves apatite formation in human bone. The inter-tubular spacing decreases as the surface roughness increases, while it increases as the annealing temperature increases, while annealing temperature increases the inter-tubular spacing.

Table 7 Surface roughness and diameter for anodized Ti−7.5Mo alloy at different annealing temperatures

Voltage/V	Time/h	Annealing temperature/°C	Diameter of surface oxide/nm	Surface roughness (R_a)/nm	Ref.
20	24	450	60	85	[123]
20	24	600	80	73	[123]

4.2.4 Surface wettability

Surface wettability is a property that defines the absorption on the surface of a material. Wettability of a specific surface is always described in two ways, i.e., hydrophilic that describes the surface's attraction to water, and hydrophobic that describes the surface's repellence to water. Higher absorbance for the Ti alloy surface oxide is required for protein absorption, which will improve new bone cell growth. Thus, hydrophilic properties with a low water-contact angle (< 62°) are preferred [124]. The contact angle of medium droplets resting on the surface is a simple way to express the wetting characteristics of a surface. As well as the hydrophilic nature of the nanotube, INDIRA et al [119] observed super wettability in water contact-angle measurements. The hydrophilic nature can be attributed to the capillary effect of the nanotubes. Due to the capillary effect, the water droplet can be rapidly absorbed into the pores of the tubes, which caused the contact angle to be reduced. Wettability improved, such as low contact angle, leads to higher surface energy, which is one of the key factors in achieving better cell adhesion process.

It has been demonstrated that the larger the diameter of the tubes, the greater the absorbance of the liquid [125]. The increased water wetting angles with pore diameters will have a significant impact on cell adhesion to the nanotube-containing surface. Cells prefer to attach to hydrophilic surfaces over hydrophobic surfaces [119]. This is due to the hydrophilic surface's ability to form a reaction with water molecules, whereas the hydrophobic surface repels water molecules. As a result, when the liquid penetrated the surface oxide nanotubes, the tube diameter increased, resulting in an increase in hydrophilic surface. It can be correlated to the applied voltage as the tube diameter increases with anodic voltage [126]. Therefore, as anodic voltage increases, the water contact angle or hydrophilic properties decrease.

4.2.5 Adhesion strength of surface oxide layer

It is well known that porous surface oxide layers, or in this case, TiO_2 nanotubes, are quite fragile in their as-anodized state. After anodization, the film grown on the titanium substrate can spontaneously peel off [127]. This is due to the anodic film's poor adhesion to the substrate, which is caused by the volume difference between the

oxide and the metal substrate, as well as the presence of anions within the oxide layer. Table 8 shows some quantitative measurements of the adhesion strength of TiO_2 nanotubes grown on a Ti-based alloy as a substrate using an anodizing process.

It appears that a post-treatment with organic solvents with lower polarity could improve the adhesion of the nanotubes layer [127]. Immersion of freshly fabricated TiO_2 nanotubes in organic solvents with lower polarity, such as petroleum ether, cyclohexane, acetone, and toluene, was found to be very beneficial in strengthening the nanotubes' adhesion to the substrate. However, post-treatment of the nanotubes after they have been freshly anodized with high polarity organic solvents such as methyl alcohol, isopropyl alcohol, and *n*-butyl alcohol may result in undesirable detachment of the nanotubes from the substrate. This phenomenon is linked to the accumulation of H^+ ions at the nanotubes' ends (inner side). As the anodizing process was concluded, hydrogen ions trapped inside the tubular structure induced the formation of bubbles at the interface between nanotube layer and substrate, resulting in the instability of the nanotubes layer, which could be easily peeled off [127]. Furthermore, CRAWFORD et al [132] reported that detachment of the nanotubes layer is easy if the layer is quite thin, i.e. 230−250 nm. However, a thicker nanotube layer (greater than 600 nm) has been reported to sufficiently strengthen the nanotubes' adhesion to the substrate. This mechanism is thought to be related to the slowing of stress buildup in the porous layer as thickness is increased.

4.2.6 Biocompatibility and cytotoxicity of surface oxide layer

Cytotoxicity test is a common evaluation that is often an important indicator of biocompatibility. In cytotoxicity test, selected cell lines are cultivated in contact with the implant materials, and after a significant period of time, the proliferation (estrogenicity) and death (toxicity) rates of the cultured cells are counted [133]. Several studies have been conducted to date to determine the cytotoxicity effects of surface oxide layer (in specific: titanium oxide nanotubes). Table 9 summarises the findings regarding the biocompatibility and cytocompatibility effects of TiO_2 nanotubes grown by anodization on various Ti alloys. In general, most research studies concluded that TiO_2 nanotubular structures have excellent cytocompatibility; however, there are some contrasting findings reporting on cytotoxicity, whereby cell attachment procedure results in undesirable cell death. MICHALKOVA et al [139] reported that anodic TiO_2 nanotubes grown on cp-Ti have cytotoxic effects on healthy human embryonic kidney cells (HEK-293) and triple-negative metastatic breast cancer cells (MDA-MB-231).

Table 8 Comparison of adhesive measurement of TiO_2 nanotubes grown through anodizing process

Substrate material	Anodizing parameter	Maximum load/mN	Tip	Adhesive failure-force/mN	Ref.
cp-Ti	Voltage: 25 V; time: 20 min; electrolyte: 0.5 wt.% sodium fluoride + 2.7 wt.% sodium sulfate	20	Berkovich diamond tip	< 10	[128]
Ti−6Al−4V	Voltage: 25 V; time: 20 min; electrolyte: 0.5 wt.% sodium fluoride + 2.7 wt.% sodium sulfate	20	Berkovich diamond tip	< 10	[128]
Ti−6Al−4V	Voltage: 60 V; time: 1 h; electrolyte: 0.5 wt.% ammonium fluoride + 1 vol% deionized water + ethylene glycol; annealing at 500 °C	30000	Berkovich tips (0.05 μm-radius)	375.26 (as-anodized); 378.45 (annealed)	[129]
Ti−6Al−4V	Voltage: 60 V; time: 1 h; electrolyte: 90 vol.% NH_4F + 10 vol.% ethane-1,2-diol + water	N/A	Diamond indenter (25 μm-radius)	862 (as-anodized); 1814 (as-annealed at 500 °C)	[130]
Ti−25Nb−25Ta	Voltage: 60 V; time: 1 h; electrolyte: 0.5 wt.% ammonium fluoride + 5 wt.% deionized water + ethylene glycol $C_2H_4(OH)_2$	500	Spherical (5 μm-radius)	>500	[131]

Table 9 Summary of biocompatibility and cytotoxicity effects of TiO_2 nanotubes grown by anodization technique on various Ti-based alloys

Substrate	Anodization parameter	Type of cytotoxicity/ proliferation assessment	Cells type	Observation	Ref.
cp-Ti	Potential: 10, 15, 20 V; time: 1 and 2 h; electrolyte: 50 mL H_2SO_4+50 mL HF	Cytotoxicity assessment via MTT assay	HeLa cells	Nanotubes grown on the substrate do not show any noteworthy cytotoxicity	[134]
cp-Ti	Potential: 10 and 15 V; time: 1 h; electrolyte: (1) 0.5 vol.% HF + deionized water (2) EG+0.7 vol.% ammonium fluoride (NH_4F)+50 vol.% deionized water	Cytotoxicity assessment via LDH assay	Human dermal adult fibroblasts (HDAF) cells	Low concentrations of TiO_2 nanotubes pose toxicity effects to the cells, whereas at higher concentrations the cell viability remained on par with controls; observation with the LDH assay shows that the plasma membrane integrity is retained, showing that there is cytotoxicity effect	[135]
Ti−7.5Mo	Potential: 20 V; time: 24 h; electrolyte: water+glycerol+ 0.25 wt.% NH_4F	Cytotoxicity assessment via LDH; time: 24 h of culture	Adipose derived stem cells (ADSCs)	No cytotoxic effects	[136]
Ti−25Nb Ti−50Nb	Potential: 30, 60 V; time: 30 min; electrolyte: 5 mL deionized water + 54 mL ethylene glycol+0.4 wt.% NH_4F	Cell viability and proliferation	Human mesenchymal stem cells (HMSCs)	Nanotubes grown at the potential of 30 V (d=~40 nm) promotes better cell adhesion as compared to that of grown at 60 V (d =~100 nm); cells proliferate better on nanotubes grown on Ti−25Nb as compared to Ti−50Nb	[137]
Ti−35Nb	Potential: 20 V; time: 1 h; electrolyte: 0.3 vol.% HF	Cytotoxicity assessment via MTT assay	MC3T3-E1 cell lines (mouse pre-osteoblast cells)	The presence of TiO_2 nanotubes on Ti−35Nb substrate improves pre-osteoblast viability and considers to be cyto-compatible to the cells	[138]

This discrepancy in findings between cyto-compatible and cytotoxic poses by TiO_2 nanotubes is a major concern that has yet to be investigated. Many factors influencing compatibility, including dose (concentration and exposure time), surface chemistry, the presence of impurities and intentional or unintentional doping, the surface morphology of nanotubes (grassy surface or flat opening), and the type of cells tested [139].

TiO_2 nanotubes grown on Ti-based alloys that have been tested to be cyto-compatible may have a high potential for use in orthopaedic implants, whereas TiO_2 nanotubes that have been found to be cyto-toxic may have a chance of being used as cancer nanomedicines. Whether it is cytotoxic or cyto-compatible, Fig. 11 depicts excellent adhesion of cells proliferated on the Ti−Nb alloy substrate, demonstrating the success of growth and proliferation. Based on this figure, TiO_2 nanotubes are generally considered cyto-compatible because the cells remain viable on the surface; however, the counts vary depending on the amount of Nb added and the diameter of the nanotubes that aid in cell proliferation.

4.2.7 Corrosion resistance of surface oxide layer

Ti and its alloys have long been recognised as corrosion-resistant metals. However, once the surface has been tailored into another phase consisting of a TiO_2 surface oxide layer, it is critical to evaluate the corrosion characteristics of the specific surface oxide layer in body fluids. When evaluating the corrosion characteristics of various Ti-based alloys intended for use as implant materials, it is important to remember that different

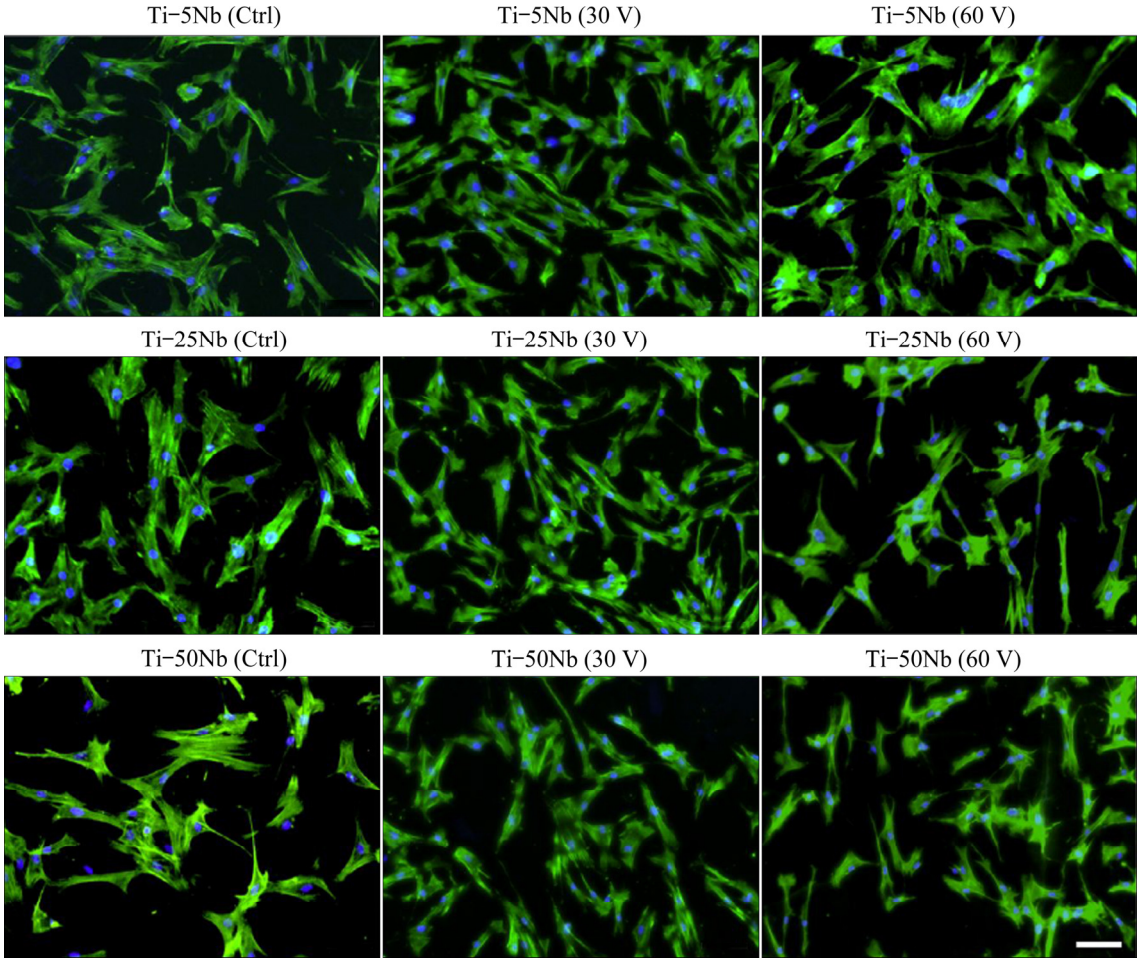

Fig. 11 Adhesion of human mesenchymal stem cells on surface of unmodified Ti−Nb substrate and nanostructured Ti−Nb substrates through electrochemical anodization: fluorescence images of cells on surface of samples after 24 h of incubation (Blue color indicates DAPI-stained nuclei, and green color indicates Alexa Fluor 488-stained F-actin (cytoskeleton) which related to their viable status. Reprinted with permission from Ref. [137]. Copyright 2020, American Chemical Society)

alloying elements in the Ti-alloys form different oxide phases on the surface after the surface modification process is completed. For example, the anodization of Ti−Nb alloys may result in the formation of TiO_2 as well as Nb_2O_3 or Nb_2O_5 [140]. Surface oxide layer mixtures play an important role in improving corrosion resistance or, in another case, preventing the release of alloying elements from the bulk alloy into body fluids [141].

A work reported by GROTBERG et al [142] examined the corrosion resistance of Ti−6Al−4V alloys and compared the corrosion tendency of the bare alloy without any surface modification with the as-anodized samples and anodized-and-annealed samples. The test used Dulbecco's Modified Eagle Medium (DMEM) supplemented with 10% fetal bovine serum as the electrolyte and was carried out at 37 °C in order to properly assess the corrosion characteristics of the anodized alloy in human physiological conditions. They concluded that anodized-and-annealed samples exhibited the greatest corrosion resistance. Annealing of the anodized samples at 600 °C for 3 h increased the corrosion potential (φ_{corr}) and lowered the corrosion current (J_{corr}), which is due to the presence of a thick and more stable anatase TiO_2 layer as compared to the thin spontaneous oxide layer for the bare alloy and non-stable amorphous oxide layer for the as-anodized oxide layer.

In another study, KONATU et al [143] looked into the corrosion resistance of Ti−15Zr alloy after it had been anodized and annealed. Anodization of the respective Ti−15Zr was carried out at a constant voltage of 20 V for 6 h in an electrolyte of glycerol containing 50% deionized water and 2.7 g/L ammonium fluoride, NH_4F. After anodization, the

samples were annealed at temperatures ranging from 400 to 650 °C. Under the electrolyte of simulated body fluid (SBF) at 37 °C, the corrosion characteristics of the samples were compared between as-anodized and as-annealed. Similar to the work reported in Ref. [144], it is discovered that the presence of nanotubes on the surface of the Ti−15Zr alloy improves corrosion resistance significantly when compared to the bare surface. In the case of as-annealed samples, because the annealing was performed within the specified temperature range, 450 °C is the best annealing temperature for this particular alloy to fit into the implant application, because this temperature converts the amorphous phase of the as-anodized samples to the state of single anatase phase, which has the best corrosion resistance when compared to rutile or a mixture of anatase and rutile.

Furthermore, TiO_2 nanotubes synthesized on the surface of the alloy with a diameter close to 80 nm and subsequently annealed at 450 °C were found to promote the best interaction between the oxide layers and adult human adipose-derived stem cells (ADSCs) [143]. This finding is consistent with the work reported by OLIVEIRA et al [145] on the corrosion resistance of Ti−Mo biomedical alloys (6 wt.% and 15 wt.% of Mo). When the corrosion tendency of anodized Ti−Mo alloys was compared to that of bare alloy, it was discovered that TiO_2 nanotubes formed on the surface of the specific alloy at 40 V for 2 to 6 h and annealed at 550 °C for 3 h were beneficial to improving corrosion resistance when tested in Ringer solution. The nanostructured surface outperformed the oxide films formed spontaneously on the bare alloy in terms of protection.

In general, when the surface of the substrate is nano-structured, the corrosion resistance improves significantly. It is quite controversial, and few studies have compared the effect of the substrate's phase on its corrosion characteristics. However, it has been discovered that Ti alloys with β phases improve corrosion resistance far more than Ti alloys with α phases (i.e. cp-Ti). This is because Ti with phase has a higher tendency to have other metal oxide phases, such as ZrO_2, TaO_2, and NbO_2 [146]. The formation of a metal oxide phase during anodization, which is stabilized during the annealing process, has potential to improve the corrosion resistance.

5 Development of surface oxide layer by surface modification methods for Ti alloys

Surface modification is required for Ti alloy implants to promote bone healing during the first days of implantation because their native surface is initially inert and takes longer to establish a bonding between the bone and the implant materials. To date, various types of surface modification methods have been investigated in order to provide a specific desirable surface for Ti alloy. Every technique utilized to modify the surface often benefits the Ti alloy substrate in their unique properties of surface topography (micron-scaled or nano-scaled), porous or dense oxide layer, surface roughness, and surface wettability, which will determine the eminence of the alloy in term of bioactivity and osseointegration when the samples are attached to living cells. Since the implant is generally regarded as foreign material at the implantation sites, it tends to be isolated from the rest of the bone tissues during the early days of implantation by the formation of fibrous tissue. This situation causes micro-movement of the implant, migration, and unexpected implant loosening. As a result, it is critical for implant materials to have good osseointegration characteristics.

Another general issue associated with implant material is the increased risk of infection due to bacterial growth. Infections following orthopaedic implant surgery have been reported in 5% of cases, amounting to 100000 cases per year in the United States alone. This issue is caused by bacterial attachment on the surface of the implant, where the bacterial colony forms a biofilm, infecting the adjacent bone and surrounding tissues. This situation not only slows the bone healing process, but also puts the implant at risk of becoming completely loose from the implantation sites [147].

Surface modification methods for titanium and its alloys are commonly classified into three groups: physical methods, mechanical methods, and chemical methods. This review would provide important insight into how surface modification methods using chemical sources, such as those listed in Fig. 12, are capable to improve the bioactivity and biocompatibility of titanium-based alloys for implant application.

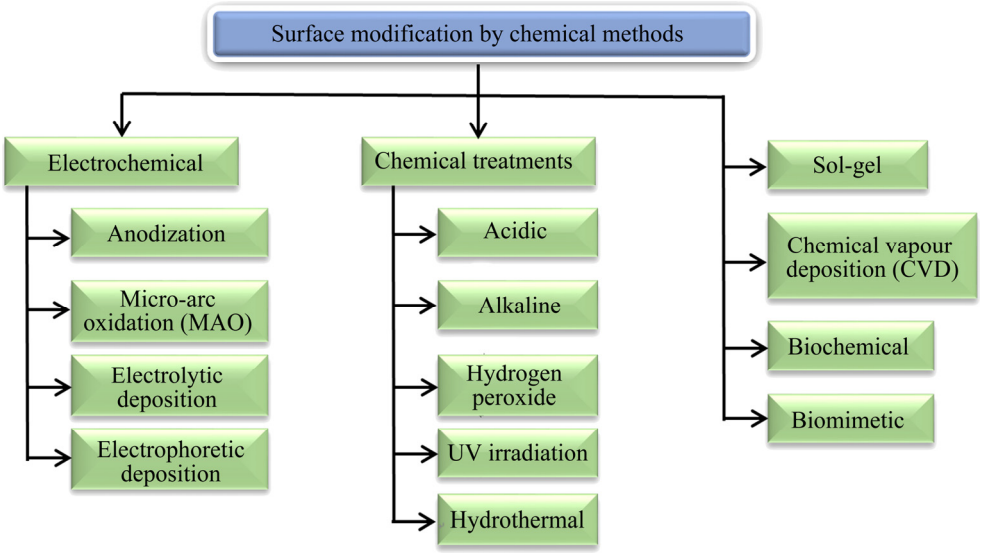

Fig. 12 Classification of surface modification methods of Ti-based biomaterials by chemical approach [148]

5.1 Electrochemical-based surface modification

5.1.1 Anodization of Ti and its alloys

Anodization, also known as anodic oxidation, is the oxidation of metal in the presence of an electric field. Ti is anodized in a two-electrode bath with Ti as the anode and an inert material as the cathode. Both electrodes are immersed in an electrolyte. Polarization causes surface oxidation and thus the formation of an anodic film when potential is applied to the anode [149,150]. The anodic film formed can be flat, but it must be porous and roughened for use in biomedical applications. As a consequence, several parameters, such as anodization voltage, time, temperature, and electrolyte selection, must be considered in this process [118,151].

There are numerous reasons why anodization is preferred for the formation of porous oxide on implant surfaces. Several reasons have been mentioned, including the ease of setup and low cost, as well as the effectiveness of the anodization process for porous oxide formation. Anodization of pure titanium is a common process for producing TiO_2, particularly in energy and catalysis applications. Through a literature search in Science Direct [152], there are 18329 scientific articles published between 2012 and 2022 reporting on anodization processes on a wide range of Ti and Ti alloys for various applications. Year after year, the number increases. Among these, there is a substantial body of work describing the formation of nanotubular TiO_2. One of the reasons for anodization is preferred over other chemical treatment methods such as micro-arc oxidation, electrophoretic deposition, sol-gel, and chemical vapour deposition is the ease with which nanotubular structures can be formed. Often, these techniques are limited to producing compact or micro-scaled structures.

The mechanism of TiO_2 nanotubular growth on pure Ti is well established and has been reviewed in detail by numerous authors, including REGONINI et al [114]. Fluoride ions must be incorporated into the anodizing electrolyte in order to form TiO_2 nanotubes with self-aligned and ordered architecture. The formation of fluoride electrolyte is generally described as occurring in three stages. The anodization process begins with the oxidation of Ti (Reaction (1)).

$$Ti \rightarrow Ti^{4+}+4e \quad (1)$$

Reaction (1) will be followed by solvatization of Ti^{4+} or reaction with oxidants such as OH^- or O^{2-} in the electrolyte to form a compact TiO_2 in accordance with a typical reaction shown in Reaction (2):

$$Ti^{4+}+4OH^- \rightarrow TiO_2+2H_2O \quad (2)$$

There is a competition between solvatization and oxide formation, which can result in the formation of porous oxide. The oxide layer can be severely dissolved by a chemical dissolution process (Reaction (3)) in the presence of fluoride ions, enlarging pores [153,154]. Pores would then

expand inwards, resulting in elongated pores. The growth front of the pores is located within the pore at the metal−oxide interface.

$$TiO_2+6F^-+4H^+\rightarrow[TiF_6]^{2-}+2H_2O \quad (3)$$

Anodization is a process that depends on the applied voltage and the movement of the ions across the growing oxide is dependent on the strength of the field developed across the anodic film. The rate of movement depends on the size of the ions, and since F^- has much smaller ionic radius than O^{2-}, it migrates faster than O^{2-} through the oxide layer. This resulted in a formation of a so-called fluoride-rich layer that accumulated at the titanium−oxide interface. Extensive research has been conducted on this process, as indicated in Fig. 13 by BERGER et al [155].

The plastic-flow of the oxide would cause the displacement of the fluoride-rich layer into cell boundaries as the pores grow. This is due to the volume difference between the oxide and the metal substrate, as well as the difference in lattice parameters. The TiO_2 can be pushed upwards in the plastic-flow mechanism to reduce stress at the titanium−TiO_2 interface, resulting in a region between two pores rich in the water-soluble fluoride compound. This compound dissolves in water, separating one pore from another, resulting in nanotubular oxide.

In essence, the anodization process for oxide formation in an alloy is the same as the anodization process for pure Ti. However, it is critical to pay close attention to the alloying element, such as the type of alloying element, distribution, and oxidation rate of the Ti alloy. From the standpoint of morphology, there have been several publications on the formation of oxide nanotubes on Ti alloys, often with success in nanotube formation when the composition is rich in Ti [143,156]. Alloy oxidation can result in the formation of mixed oxide. For example, oxidation of Ti−Zr alloy or Ti−Nb alloy can yield both TiO_2−ZrO_2 and TiO_2−Nb_2O_5 phases within a single nanotube. It is, however, also affected by the nature of the alloy substrate and the distribution of phases within the alloy. The oxide grown on each phase of a Ti-alloy such as Ti−Nb, which is composed of α and β phases, can have different morphologies and properties.

It is also worth mentioning that the presence of metal oxides such as ZrO_2 and Nb_2O_5 along with TiO_2 nanotubes showed better corrosion resistance in the Ti alloy with β-phase, as compared to that of

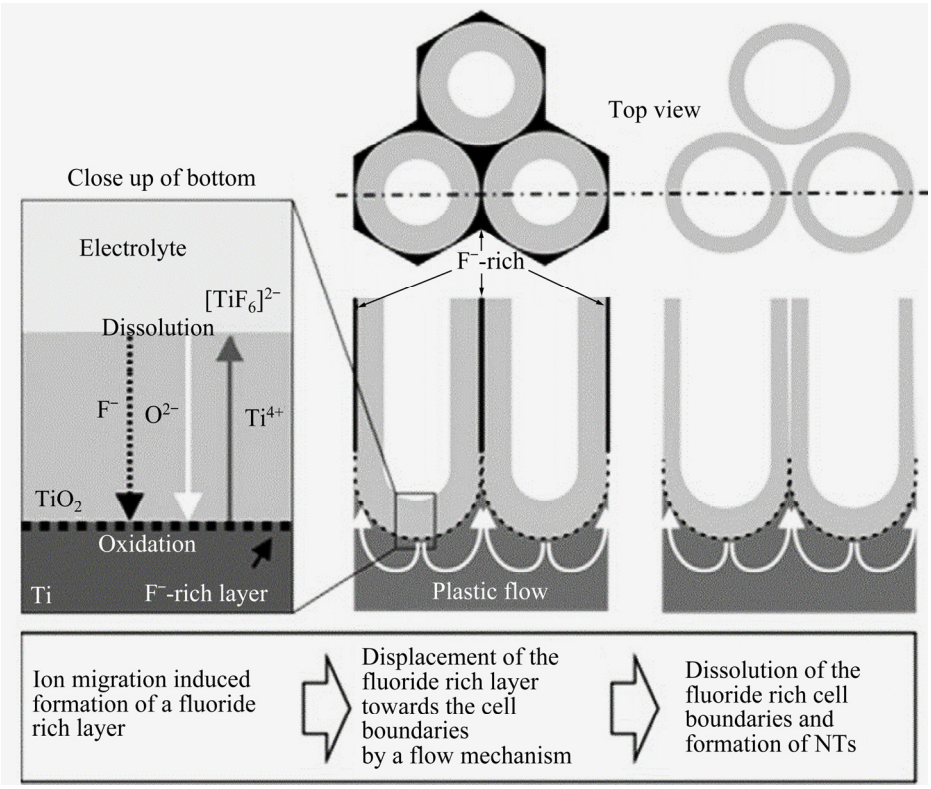

Fig. 13 Mechanism of fluoride-rich layer formation and transition from pores to tubes by dissolution of fluoride-rich layer at cell boundaries (Reprinted with permission from Ref. [155]. Copyright 2011, Elsevier)

corrosion resistance of pure Ti (α-phase) or Ti6Al4V (α-phase) alloy. The resultant oxides from the alloying elements containing β-stabilizers such as ZrO_2, Nb_2O_5 and Ta_2O_5 strengthen the TiO_2 nanotube layer with the noticeable improvement in the corrosion resistance, along with the biocompatibility of the alloys, since Zr, Nb and Ta are long known to be non-toxic and non-allergic elements [141,146,157]. In terms of the specific application to be used as an implant material, the bioactivity of other metal oxides requires further and deeper investigation because it has not been widely reported in the literature to date. For example, scientific findings reporting on the bioactivity of Nb_2O_5 as a broadly used-stabilizer in Ti alloys once it forms oxides during the anodization process are very rare. To highlight the aforementioned issue, this review uses β-type Ti alloy with Nb as an alloying element as an example.

5.1.1.1 Anodization parameters of Ti-based alloys

As previously stated, the success of nanotube formation by anodization in the case of pure Ti is dependent on anodization parameters, so have the resulting dimensions of the nanotubes, specifically their length and diameter. These dimensions can be tuned by adjusting anodization parameters such as applied voltage, anodization time, electrolyte composition, electrolyte pH, stirring, working distance, and anodization temperature. Indeed, a simple relationship can be derived from nanotubes grown on pure Ti, and the resulting nanotubes are often self-arranged with uniform length and diameter. Larger diameter nanotubes can be created simply by increasing the voltage, whereas longer length nanotubes can be created by increasing the anodization time. The morphology of an anodic film on an alloy, on the other hand, is far more complex. As previously stated, the success of nanotube formation on an alloy is determined by the alloy's composition, phases, phase distribution, grain size, and the nature of the grain boundaries. Nanotubes formed on Ti alloys are commonly not as uniform as pure Ti, with diameter and length variations depending on the properties of the alloys from underneath. Among the various alloys being investigated, anodization of Ti−Nb is particularly intriguing, as shown in Table 10. Several important anodization parameters are shown here, as well as the dimensions of the TiO_2 and bioactivity properties of the anodized alloy.

5.1.1.2 Effect of anodization potential

The anodization potential determines the electric field strength across the oxide, which influences ion migration and, eventually, nanotube diameters. The applied voltage has a direct effect on pore diameter and anodic film thickness (nanotubes length). The higher the applied voltage is, the larger the nanotube diameter is and the longer the nanotubes are. Figure 14 depicts an observation on the effect of anodization voltage on pure Ti nanotube diameter, which supports the aforementioned trend.

Smaller nanotube diameters are preferred for implant applications due to improved bone-to-cell adhesion. Clearly, BRAMMER et al [125] and TAN et al [112] reported a case study of apatite-growth in anodized cp-Ti with different nanotube diameters of 30, 50, 70, and 100 nm, with the smallest diameter, 30 nm, exhibiting the highest degree of cell adhesion. Another finding is that cell adhesion, alkaline phosphatase (ALP) activity, and initial bone mineralization on anodized Ti are increased with nanotube diameters ranging from 20 to 70 nm. However, as the diameter of the TiO_2 nanotubes increased beyond 70 nm, cell adhesion decreased until it reached the lowest point at 120 nm [163].

There is a minimum voltage at which nanotubes can be fabricated by anodization. This minimum voltage is affected by the electrolyte used. The minimum voltage in a buffered or aqueous fluoride electrolyte is often 10 V. There is also a maximum voltage above which the nanotubular structure degrades. The maximum voltage in a buffered or aqueous electrolyte is around 30 V. However, in organic electrolytes, the maximum voltage can reach 120 V, depending on the exact nature of the electrolyte used. As a result, larger diameter nanotubes can be produced in organic electrolytes. For the formation of 80−100 nm diameter nanotubes in organic electrolytes, the applied voltage is typically in the range of 50 to 60 V. For nanotubes with smaller diameters, a voltage of 20−40 V can be used.

CHERNOZEM et al [137] investigated the effect of niobium content in Ti alloys and voltage variation on the morphology of anodic oxide formed (Table 10). An alloy containing 5 wt.% Nb can produce nanotubes with a diameter of 56 nm under constant voltage of 30 V and anodization time of 30 min. Increasing the Nb to 25 wt.% and

Table 10 Important parameters of anodization on Ti−Nb-based binary alloys

Composition/ wt.%	Parameter of anodization			Significant findings			Ref.
	Electrolyte	Applied potential and time	Post-treatment	Phase of oxide layer	TiO_2 nanotube characteristic	Bioactivity evaluation	
Ti−5Nb	0.4 wt.% NH_4F+ 54 mL EG+ 5 mL DI	Potential: 30, 60 V; time: 30 min	Annealing at 500 °C in air for 3 h	Anatase + α'-Ti	TiO_2 nanotubes are vertically aligned on surface of Ti−Nb alloys; diameter=56 nm (30 V); diameter=80 nm (60 V); length=0.75 μm (30 V); length=3 μm (60 V)	Nanotubes grown at 30 V with diameter of 56 nm showed the best human mesenchymal stem cells (hMSC) after adhesion for 24 h	[133]
Ti−10Nb	1.0 mol/L Na_2SO_4+ 0.1 wt.% HF	Potential: 20 V; time: 40 min	N/A	Anatase	α-phase: self-organized TiO_2 nanotubes with random diameters; length=0.59 μm β-phase: lamellar structure; length=1.36 μm	N/A	[158]
Ti−10Nb	1.0 mol/L H_3PO_4+ 0.8 wt.% NH_4F	Potential: 20 V; time: 40 min	Annealing at 230, 430, and 530 °C for 3 h	Anatase + Nb_2O_5	α-phase: self-organized TiO_2 nanotubes with random diameters; length=0.82 μm β-phase: lamellar structure; length=1.53 μm	N/A	[140]
Ti−10Nb	1.0 mol/L H_3PO_4 + 0.8 wt.% NaF	Potential: 10 V; time: 2 h	N/A	N/A	Highly self-organized TiO_2 nanotubes; diameter ranging from 55 nm (small tubes) to 220 nm (large tubes); length=730 nm	N/A	[159]
Ti−20Nb	1.0 mol/L H_3PO_4 + 0.8 wt.% NaF	Potential: 10 V; time: 2 h	Annealing at 300, 450, and 600 °C (annealing time was not specified)	TiO_2 annealed at 300 and 450 °C: anatase; TiO_2 annealed at 600 °C: anatase + rutile	Highly self-organized TiO_2 nanotubes diameter ranging from 55 nm (small tubes) to 220 nm (large tubes); length=940 nm	N/A	[159]
Ti−25Nb	0.4 wt.% NH_4F + 54 mL EG + 5 mL DI	Potential: 30, 60 V; time: 30 min	Annealing at 500 °C in air for 3 h	TiO_2 anodized at 30 V: anatase + α''-Ti + β-Ti; TiO_2 anodized at 60 V: anatase + α''-Ti	TiO_2 nanotubes are vertically aligned on surface of Ti−Nb alloys; diameter=50 nm (30 V); diameter=100 nm (60 V); length=1.5 μm (30 V); length=10 μm (60 V)	The highest proliferation of human mesenchymal stem cells (hMSC) on nanotubes grown at 30 V with inner diameter of ~50 nm after10 d of incubation	[137]

(to be continued)

Composition/ wt.%	Parameter of anodization			Significant findings			Ref.
	Electrolyte	Applied potential and time	Post-treatment	Phase of oxide layer	TiO_2 nanotubes characteristics	Bioactivity evaluation	
Ti−30Nb	1.0 mol/L H_3PO_4 + 0.8 wt.% NaF	Potential: 10 V; time: 2 h	N/A	N/A	Highly self-organized TiO_2 nanotubes diameter ranging from 55 nm (small tubes) to 220 nm (large tubes); length=1.5 μm	N/A	[159]
Ti−40Nb	1.0 mol/L H_3PO_4 + 0.8 wt.% NaF	Potential: 10 V; time: 2 h	N/A	N/A	Highly self-organized TiO_2 nanotubes diameter ranging from 55 nm (small tubes) to 220 nm (large tubes); length = 2 μm	N/A	[159]
Ti−45Nb	0.05 mol/L $NaClO_4$ + 0.05 mol/L NaCl in 50:50 vol.% of H_2O:C_2H_5OH	Potential: 40 V; time: 2 min	Annealing at 700 °C in air for 3 h	Anatase + rutile + mixed Ti−Nb-oxides ($TiNb_2O_7$; $Ti_2Nb_{10}O_{29}$; $3Nb_2O_5/TiO_2$)	Nanotubes are randomly oriented but individual morphology and nanotube diameter is much more uniform; diameter=20−100 nm; length=50 μm	N/A	[160]
Ti−45Nb	1.0 mol/L $(NH_4)_2SO_4$ + 0.25 mol/L NH_4F	Potential: 10−60 V; time: 10−480 min	N/A	N/A	Nanotubes with bimodal morphology; larger diameter= 86−336 nm; Smaller diameter=57−185 nm; length=200 nm−5.2 μm; below 15 V and above 55 V, large and small tubes still exist but no more well self-organized (randomly distributed)	N/A	[161]
Ti−50Nb	0.4 wt.% NH_4F+ 54 mL EG+ 5 mL DI	Potential: 30, 60 V; time: 30 min	Annealing at 500 °C in air for 3 h	TiO_2 anodized at 30 V: anatase + rutile + β-Ti; TiO_2 anodized at 60 V: anatase + β-Ti	TiO_2 nanotubes are vertically aligned on surface of Ti−Nb alloys; diameter=54 nm (30 V); diameter=108 nm (60 V); length=1.3 μm (30 V); length=15 μm (60 V)	Human mesenchymal stem cells (hMSC) did not adhere and proliferated very well on nanotubes grown at 30 and 60 V due to larger diameter of NTs (more than 50 nm) as well as effect of high content of Nb (50 wt.% Nb). Both factors lead to cell detachment	[137]

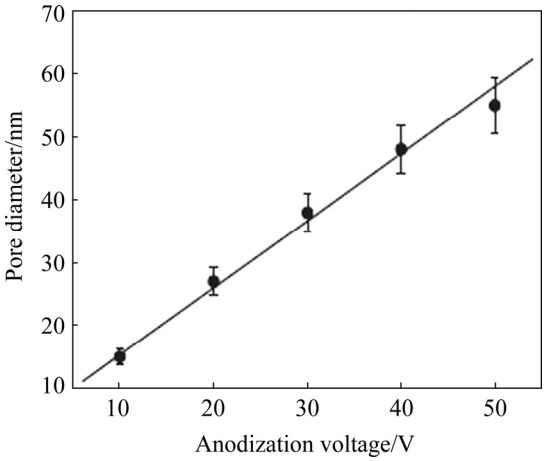

Fig. 14 Effect of anodization voltage on nanotubes diameter of commercially pure Ti (cp-Ti) (Reprinted with permission from Ref. [162], Copyright 2014, Elsevier)

50 wt.% increases the diameter to 50 and 54 nm, respectively. Increasing the anodization potential to 60 V resulted in larger diameter nanotubes of ~108 nm on Ti with 50 wt.% Nb addition. As a result, it is clear that the content of the alloying element and the voltage are important parameters in determining the size of the nanotubes formed. The length of nanotubes is also related to the voltage applied and the content of Nb added.

When tested on the human mesenchymal stem cells (hMSC), nanotubes with a diameter of 50 nm appear to have the best adhesion and proliferation [137]. Cells cannot bind properly when the nanotubes are larger in diameter [164]. Furthermore, the cell is affected by the amount of Nb in the alloy. Cell adhesion and proliferation were found to be the lowest when the addition of Nb is >50 wt.%. To achieve a nanotube diameter of ~50 nm, anodization must be performed in a lower voltage range.

JANG et al [159] have reported the effect of Nb addition in Ti−Nb alloys system on the length of nanotubes formed. Anodization of 10 wt.% Nb addition in Ti−Nb alloys system is said to result in nanotubes with length of 730 nm. As the Nb content was increased up to 40 wt.%, the nanotubes were 2 μm in length (10 V for 2 h). The TiO_2 nanotubes were highly self-organized with the diameter ranging from 55 to 220 nm.

5.1.1.3 Effect of anodization time

Another important factor in controlling the morphology of nanotubes is the anodization time. The anodization time, in particular, is directly related to the length of the nanotubes growth as well as adequate surface etching for clear opening of the nanotubes. Oxide formation occurred within a few seconds of polarisation in an early anodization process [165]. Since the oxide is thin, it can be easily etched in the presence of fluoride ions or by electric field dissolution, resulting in small pits. The evidence in Fig. 15 shows that as the anodization time increased, the nanotubes became more well-defined. At shorter anodization time, the surface oxide is composed of small pits and a random porous structure. An hour of oxidation is regularly sufficient for good surface opening of nanotubes [166]. However, this effect is limited because, after a prolonged anodization time, the

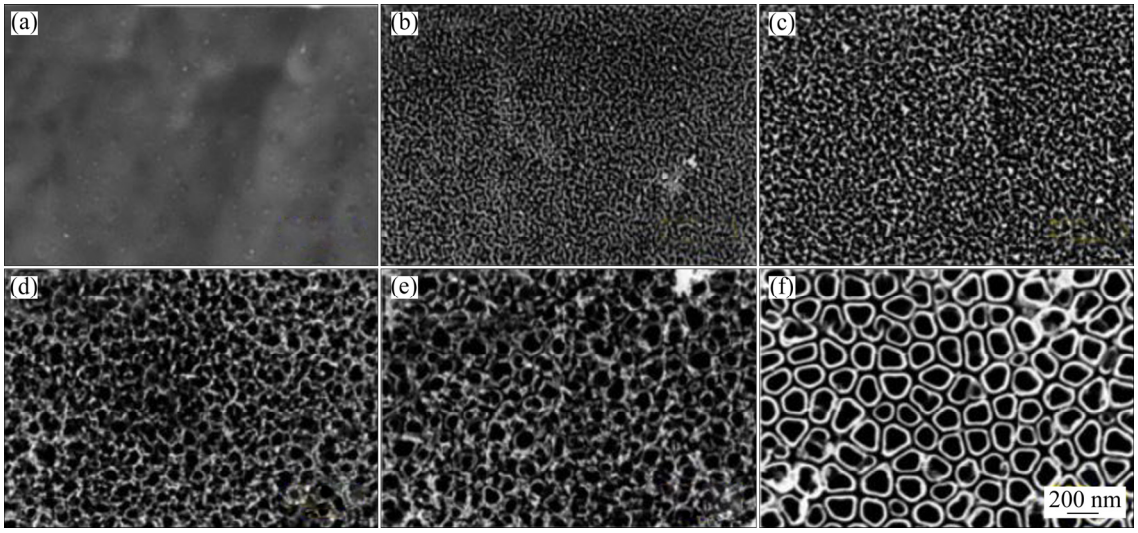

Fig. 15 FESEM micrographs of Ti−6Al−7Nb alloys anodized at various time: (a) 12 s; (b) 5 min; (c) 10 min; (d) 15 min; (e) 30 min; (f) 60 min (Reprinted with permission from Ref. [166]. Copyright 2020, Elsevier)

nanotubes are chemically etched, resulting in the formation of thinned surface oxide [115].

In Table 10, FENG et al [161] investigated the effect of anodization time (10, 20, 60, and 480 min) on the formation of TiO_2 nanotubes on Ti−45Nb alloys at 40 V. After 60 min of anodization, the average diameters of both large and small diameter nanotubes will become more consistent. Another finding from Table 10 is that TiO_2 nanotube formation is nearly complete after 1 to 2 h of anodization, depending on the type of electrolytes used. Less viscous electrolytes typically contribute to a shorter anodization time, whereas higher viscosity electrolytes generally require a longer time to form satisfactorily grown TiO_2 nanotubes.

5.1.1.4 Effect of types of electrolytes

Anodization in fluoride electrolyte is often used for the successful formation of TiO_2 nanotubes, with the amount of fluoride added ranging from 0.2 to 0.7 wt.% [167,168]. Fluoride sources include KF, NH_4F, and NaF. A so-called first generation electrolyte used acidic solution, resulting in short nanotubes due to excessive surface etching [114]. This is followed by a second generation electrolyte based on a buffered electrolyte such as Na_2SO_4, with longer nanotube formation but serration on the nanotube walls. In recent years, anodization has been performed in organic electrolyte, allowing nanotubes formed in this third-generation electrolyte to be longer with smoother walls. Glycerol and ethylene glycol are examples of electrolytes. However, an adequate oxidant is required, so water is frequently added to electrolytes [119]. As previously stated, voltage effect is also dependent on anodization electrolyte, with organic electrolyte producing nanotubes with diameters reaching 200 nm under high applied voltage (~80−100 V), whereas buffered electrolyte produces nanotubes with a diameter around 80 nm under high applied voltage (~30 V). The main distinction between the three generations of electrolytes is the polarity and viscosity of the liquid. The latter had a significant impact on ion mobility and, as a result, the oxide growth mechanism. Growth in organic electrolytes is more balanced, resulting in nanotubes with constant length, relatively smooth walls, and good surface etching [115,119].

There is also a concern on the use of fluoride electrolyte for nanotubes formation. KULKARNI et al [115] reported that self-organized TiO_2 nanotubes morphology is commonly observed when the anodization is performed in fluorine-based electrolytes, but non-fluorine-based electrolytes such as ($NaClO_4$+NaCl+H_2O+C_2H_5OH) [160], (NaCl+H_2O+glycerol) [169], (KBr+H_2O+glycerol) [170], and ($HClO_4$+$NaClO_4$) [170] also can be used. When other non-fluoride electrolytes are used, however, uniformity in TiO_2 nanotube size and thickness remains a major challenge.

5.1.1.5 Effect of electrolyte pH

The pH of the electrolyte is also an important factor in the success of nanotube formation and control over the diameter and length of the nanotubes formed. The pH of the solution has a significant impact on the rate of oxide dissolution, which controls the pore diameter and surface etching. Nonetheless, the pH effect is also affected by the electrolyte used, with aqueous electrolytes being more noticeable than organic electrolytes. When the electrolyte has a very low pH of 1−3 [171,172], the dissolution rate in aqueous acidic electrolyte is high. The nanotubes formed in this electrolyte are quite short. The pH of the buffered electrolyte is typically in the range of 6−7, and the resulting nanotubes are frequently longer. Increasing the pH > 8 in such an electrolyte would obstruct the formation of nanotubes. Despite the fact that organic electrolyte such as ethylene glycol has a pH between 8 and 9, nanotubes are successfully formed even without pH reduction. Additionally, organic electrolytes can generate extremely long nanotubes [171].

5.1.1.6 Effect of anodization temperature

The electrolyte can be heated during the anodization process to speed up the reaction. Higher electrolyte temperatures can result in less viscous electrolyte, which leads to a faster etching rate, and the oxide layer dissolves faster, forming pores [119]. Although some studies reported temperatures ranging from 0 to 40 °C [114,126], nanotubes can be formed in electrolyte at 20−25 °C (room temperature). At temperatures above 40 °C, the nanotubular structure is more often destroyed, resulting in an irregular porous structure. Due to the slower etching rate, anodizing temperatures that are too low can result in irregular pores [115]. As a consequence, room temperature is sufficient for the

formation of nanotubes on Ti or Ti-alloys.

5.1.1.7 Apatite forming ability on TiO_2 nanotubes structure

The formation of bone-growth-related materials such as calcium phosphate mineral ($Ca_{10}(PO_4)_6(OH)_2$ is an important feature for orthopaedic and dental implants. Immersion in SBF causes in vitro apatite formation and is also used as an indicator of a material surface's in vivo bioactivity. In general, their in-vitro-bioactivity can be assessed based on the formation of apatite after soaking in SBF for a specific period of time (e.g., 7, 14 d) [117]. Evidently, the findings of BAI et al [117] and TSUCHIYA et al [172] reported that annealed Ti alloys (with anatase or a mixture of anatase and rutile phase) with surface oxide nanotubes have greater ability to promote the nucleation of apatite than that of amorphous structure of nanotubes.

Since it is well known that the diameters have a significant impact on bioactivity or cell adhesion and proliferation on TiO_2 nanotubes, many studies in the field have reported discrepancies in their reported values of nanotube diameters. WANG et al [124] reported that the smaller diameter of nanotubes (70−80 nm) is more advantageous due to higher ion diffusion effects (such as Ca^{2+} and PO_4^{3-} ions from SBF). A large number of Ca^{2+} ions and PO_4^{3-} ions would penetrate the nanotubes, forming a thin Ca−P layer and promoting the formation of apatite nuclei. Cell adhesion and proliferation on TiO_2 nanotubes grown on Ti−Nb alloys were the most effective when the nanotubes were smaller than 50 nm in size, according to CHERNOZEM et al [137]. A similar study on the osteoblast cell activity of TiO_2 nanotubes grown on cp-Ti revealed that the nanotubes with the greatest degree of cell adhesion have a diameter of 30 nm [125]. According to these reports, it is quite difficult to determine the ability of TiO_2 nanotubes when it is simulated, whether in in-vitro evaluations (indicator: apatite forming ability) or in-vivo tests (direct testing in living animals). However, it can be a useful guide that the apatite nucleates and the cells proliferate to the best state under the smaller size of TiO_2 nanotubes. It is worth noting that, in addition to the size of the nanotubes, the length and thickness play an important role in determining bioactivity. Thicker nanotubular layers (i.e. (1291±5) nm) are unfavourable to diffusion due to the longer dispersal distance and low diffusion rate of elements [116]. As a result, the optimal thickness of the nanotubular oxide layer is suggested to be 3−7 nm [173]. Based on these findings, it can be concluded that the Ti alloy with surface oxide nanotube layers is unquestionably capable of enhancing apatite formation when compared to the bare surface [172].

5.1.2 Micro-arc oxidation (MAO)/plasma electrolytic oxidation (PEO)

Micro-arc oxidation, also known as plasma electrolytic oxidation (PEO) and micro-plasma oxidation (MPO), is a surface modification technology that is used to create multiple and thick ceramic-based coatings on the surfaces of light metals and their alloys [174−176]. Essentially, the MAO or PEO process requires an electrolyte bath of a dilute aqueous solution, with some additives added to customize the surface coating's properties. This technique is preferred because the coating can be tailored, for example, the addition of dopant elements can be easily incorporated by having them in the electrolyte. The MAO process is carried out at extremely high potentials ranging from ~250 to 750 V. Such a high potential can generate plasma on the surface of the substrate, resulting in the formation of a coating. Despite the fact that MAO is said to be a more complex process than anodization and other coating procedures [176], it can be used to produce thick coating. High temperatures combined with plasma pressure would result in crystalline oxide with thicknesses ranging from tens to hundreds of microns, depending on the electrical parameters and electrolytes. Thick coating often benefits the substrate in terms of wear and corrosion resistance in some applications [175].

The MAO process is divided into three steps. The first step is to rapidly increase the voltage, allowing a thin protective oxide layer to form on the substrate surface. The second step occurs when the applied voltage reaches a critical value, resulting in dielectric breakdown and micro-spark discharge. The discharge of the micro-spark partially destroys the oxide layer, triggering the formation of the porous oxide layer. In the final step, a voltage drop to negative values causes cooling of the oxidized substrate or rapid quenching of coated areas [109].

The growth mechanism and resultant properties of the protective coatings fabricated by the MAO method, on the other hand, are not as

straightforward because they are influenced by a variety of factors, including the substrate chosen, the time of the process, the power mode and other electrical parameters, and the electrolyte's characteristics, including its temperature and the additive materials added to the electrolyte. However, the electrolyte has the greatest impact on the coating. LI et al [174] used three different types of electrolytes to treat the surface of Ti−6Al−4V alloy: silicate, phosphate, and mixed silicate and phosphate electrolytes. They concluded that when silicate electrolyte was used, the MAO coating structure was porous and had poor adhesion, whereas phosphate electrolyte resulted in a compact coating structure with high adhesion strength between the substrate and the coating layer. This behaviour could be attributed to the fact that the silicate-based electrolyte has a higher tendency to deposition than the phosphate-based electrolyte, which increases the roles of surface discharges as the coating grows.

Another distinction of MAO technology over other coating or surface modification technologies is the formation of a double-layer coating structure with a dense inner layer and a porous outer layer. Table 11 shows that how various coating additives can be incorporated into the electrolytes in MAO. Additives can improve coating strength, corrosion and wear resistance, as well as antibacterial resistance. Silver (Ag), copper (Cu), and zinc (Zn) are commonly used for the latter. Aside from the common choices of Ag, Cu, and Zn to impart antibacterial resistance to MAO-coated titanium alloys, it has been reported that fluoride content in sodium fluoride (NaF)-containing electrolyte can also impart the excellent antibacterial properties and improve the osteogenic activity [183]. The MAO process is generally regarded as a non-hazardous process, capable of coating parts with complex shapes and large surfaces, and the majority of the

Table 11 Various Ti-based alloys coated through micro-arc oxidation and their biocompatibility assessment

Substrate	MAO treatment condition		Property of MAO coating layer			Ref.
	Electrolyte	Process parameter	Phase composition	Thickness/ μm	Biocompatibility assessment	
Ti−6Al−4V	Phytic acid + KOH + EDTA-$CuNa_2$ + EDTA-$ZnNa_2$	Pulse frequency: 2000 Hz; current density: 110 mA/cm^2; treatment time: 3 min; duty cycle: 35%	Cu_2O and $Zn_3(PO_4)_2$	N/A	Treated samples showed excellent cytocompatibility when tested on MG63 cells; treated samples showed superior antibacterial properties when tested against 3 bacteria (*MRSA, E.coli*, and *S.aureus*)	[177]
Ti−6Al−4V	Nano-HA + graphene nanosheets (GNS)	Pulse frequency: 1000−2000 Hz; positive voltage: 500 V; negative voltage: 100 V; treatment time: 10 min; duty cycle: 10%	Anatase-TiO_2; rutile-TiO_2; hydroxyapatite TCP; α-Ti; β-Ti	3.9−18.8	N/A	[178]
Ti−6Al−4V	0.02 mol/L β-glycerophosphate disodium (β-$GPNa_2$) + 0.2 mol/L calcium acetate ($Ca(CH_3COO)_2·H_2O$) + (5 mg/50 mg) of nano-Ag	Pulse frequency: 1000 Hz; current density: 80 mA/cm^2; treatment time: 3 min; duty cycle: 10%	Anatase-TiO_2; rutile-TiO_2; hydroxyapatite	N/A	Treated surface showed superior antibacterial properties when tested against *P.gingivalis* bacterial colony; treated surface showed good biocompatibility over attachment with mouse fibroblast cell (L929)	[179]

(to be continued)

Substrate	MAO treatment condition		Property of MAO coating layer			Ref.
	Electrolyte	Process parameter	Phase compositions	Thickness/ μm	Biocompatibility assessment	
Ti−13Nb−13Zr and Ti−45Nb	Dilute aqueous sodium phosphate (0.05 mol/L $Na_3PO_4·12H_2O$)	Pulse frequency: 50 Hz; current density: 10 mA/cm^2; treatment time: 2, 5 and 10 min	N/A	N/A	Treated substrates showed evidence of apatite mineral deposition, without restricting osteoblast activity or introducing any undesirable inflammatory responses upon culturing with foetal human osteoblasts (fHOb) cells	[180]
Ti−15Mo	0.1 mol/L $Ca(H_2PO_2)_2$ + tricalcium phosphate; 0.1 mol/L $Ca(H_2PO_2)_2$ + wollastonite; 0.1 mol/L $Ca(H_2PO_2)_2$ + silica	Current density: 100 mA/cm^2; treatment time: 5 min; voltage: 150, 200, 250, 300 and 350 V	Anatase-TiO_2; rutile-TiO_2; B-$Ca_2P_2O_7$	1.25−6.70 (in TCP-containing electrolyte); 3.40−4.60 (in $CaSiO_3$-containing electrolyte); 2.75−4.50 (in SiO_2-containing electrolyte)	N/A	[181]
Ti−25Nb−3Zr−2Sn−3Mo	0.04 mmol/L β-glycerophosphate + 0.2 mmol/L calcium acetate + deionized water	Voltage: 350 V; pulse frequency: 50 Hz; duty ratio: 50%; treatment time: 5 min	Anatase-TiO_2; rutile-TiO_2; HA; $CaTiO_3$	N/A	Implantation of the treated samples in femoral canal of 12 adult dogs (in-vivo evaluation) showed significant improvement in bone-to-implant contact	[182]

electrolytes used in this process are naturally environmentally friendly basic electrolytes [184]. Figure 16 depicts a basic comparison of the MAO and anodization processes.

5.1.3 Electrophoretic deposition (EPD)

EPD is a preferred electrochemical process for coating intended for biomedical applications as it offers a possibility of many different types of coating. It is a colloidal processing technique that works based on two different steps: (1) electrophoresis in which charged particles in a suspension are made to move towards an oppositely charged substrate under an electric field, and (2) deposition process where the particles coagulated to create a homogeneous and coherent coating layer on the surface of the conductive substrate [149].

EPD is considered a versatile and cost effective coating technique of a metallic component. Bioactive coating by EPD is found to be stable and homogeneous with uniform grain size. The coating has significant enhancement in mechanical and chemical properties [186]. The most important parameters to be controlled in EPD process are the potential and time, as well as the pH or stability of the suspensions. These parameters will determine the thickness, homogeneity, adhesive property and roughness of the coating layer.

According to a study published by MOSKALEWICZ et al [187], in order to produce thick multi-component EPD coating, suspension stability or pH must be prioritised. The particles to be coated on the surface of the substrate must be carefully suspended in a suitable dispersing medium, with some additives functioning to prevent powder agglomeration or changes in zeta potential (ZP) and particle surface potential. In the study, a composite coating of Si_3N_4/polyetheretherketone (PEEK) was successfully deposited on a Ti−13Nb−13Zr substrate. The suspensions were made with two types of solvents: isopropanol-based and ethanol-based, with chitosan or branched polyethylenimine (PEI) added as a dispersant. It was discovered that using an isopropanol-based suspension with the addition of PEI caused

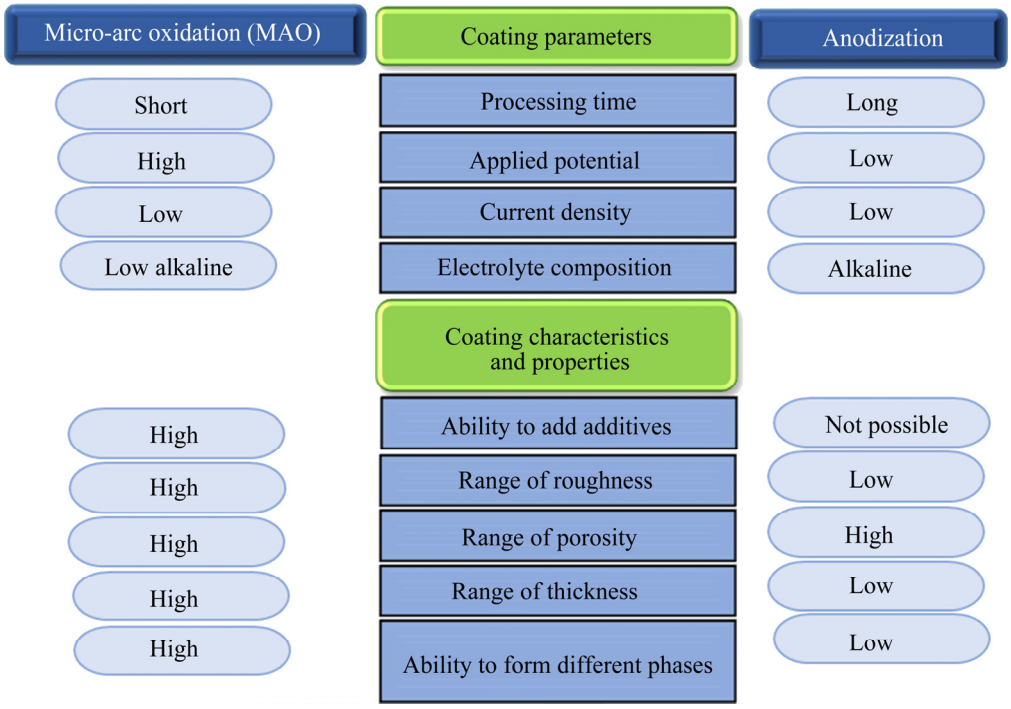

Fig. 16 Comparison between MAO and anodizing coating methods on titanium-based substrates [185]

inhomogeneity on the coating surface, with visible agglomerations of Si_3N_4 nanoparticles and PEEK particles. Furthermore, increasing the pH of the suspensions to more than 6.5 (with the addition of a base in higher concentration) causes the suspension to be highly unstable, preventing zeta potential measurement. Table 12 shows the properties of the resultant coating layer for several Ti-based alloys that have undergone electrophoretic deposition.

5.2 Chemical treatment

5.2.1 Acidic treatment

Acidic treatment is a method of removing unwanted contamination from a metal surface, resulting in a clean and uniform surface finish. Several types of acids are combined in acid treatment to produce mixed etchant, and alkaline solution is sometimes added as well. Strong acids, such as hydrofluoric acid (HF), can etch the native oxide layer on the surface of Ti alloys, forming soluble titanium fluorides and hydrogen. When Ti is exposed to hydrogen, it usually results in hydrogen embrittlement, which is undesirable because it reduces the surface properties. As a result, the most important criterion in this type of treatment is the proper acidic solution selection and concentration [192]. TAKEUCHI et al [193] investigated the effectiveness of three acids in removing contamination from the surface of commercially pure Ti: sodium peroxodisulfate ($Na_2S_2O_8$), sulfuric acid (H_2SO_4), and hydrochloric acid (HCl). In comparison to the other two acids, they concluded that a mixture of 10.0 mol/L HCl and acetone was the best decontamination agent. HCl could easily form Ti salts while not weakening the Ti surfaces.

Acid treatment is typically used in conjunction with other treatment methods to further tailor the surface properties of Ti alloys, such as improving biocompatibility and corrosion resistance. For example, ESCOBAR et al [194] reported the surface treatment of Ti−12Mo−6Zr−2Fe (TMZF) alloys with HCl followed by alkaline sodium hydroxide (NaOH) solution (acid-and-alkali-treatment). They compared acid-and-alkali-treated alloys to anodize Ti alloys with TiO_2 nanotubes formed on their surfaces. They discovered that anodized alloy had lower corrosion resistance than acid-and-alkali-treated alloy. A thin layer of protective oxide on the surface is responsible for the lower corrosion resistance of acid-and-alkali-treated TMZF. ZHAN et al [195] conducted another comparison study in which Ti−24Nb−4Zr−8Sn alloys were surface modified using a combination of sand-blasting and acid treatment. The acid treatment was carried out in a solution of sulfuric

Table 12 Basic parameters of electrophoretic deposition (EPD) of several Ti-based alloys

Substrate	Coating material	Preparation of suspension	Electrophoretic deposition parameter	Properties of coating	Ref.
cp-Ti	BG + HA (in whiskers form)	Solvent: isopropanol; dispersant: TA	Cathode: cp-Ti substrate; anode: stainless; steel plate time: 1 min; potential: 40 V	Finer particle size of BG greatly improved the bioactivity and antibacterial characteristics; combination of HA and BG improves capability to generate apatite layer (in 3 d)	[188]
Ti−6Al−4V	HA + TiO_2	Solvent: absolute ethanol; dispersant: iodine	Cathode: Ti−6Al−4V substrate; anode: 316L stainless steel; time: 3 min; potential: 20 V	Addition of TiO_2 minimizes the porosities; coating of HA and TiO_2 improves the corrosion resistance; the coating accelerates the apatite formation, owing to its improvement in wettability	[189]
Ti−6Al−4V	HA + Cu	Solvent: isopropanol; dispersant: TA	Cathode: Ti−6Al−4V substrate; anode: graphite; time: 10 min; potential: 50 V	The structure of the coating is porous due to agglomeration of Cu nano-sized particles; 3 wt.% of Cu with the HA showed the best cytocompatibility when tested in-vitro with MG63 cells; the presence of Cu in the coating increases antibacterial resistance when tested against *E.coli* and *S.aureus* bacterial colonies	[190]
Ti−6Al−4V	PEEK	Solvent: ethanol; dispersant: N/A	Cathode: 316L stainless steel; anode: Ti−6Al−4V substrate (anodic EPD); time: 20 s; potential: 10−110 V	Post-treatment of the coating layer after EPD process changed the amorphous phase to semi-crystalline phase (post-treatment: 380 °C for 20 min); a homogeneous, dense and continuous PEEK coatings on the Ti−6Al−4V substrate improved the wear resistance and micromechanical performance	[191]

BG: Bioactive glass; Cu: Copper; HA: Hydroxyapatite; TA: Triethanolamine; PEEK: Polyetheretherketone

acid and hydrochloric acid. They found that anodized alloys performed better in terms of new bone formation (osteogenesis) than sand-blasted and acid-treated alloys.

Acidic treatment is typically used as a pre-treatment process to clean the surface of the respective Ti alloys prior to the next surface modification process. Acid treatment alone is insufficient to tailor the surface and meet the various requirements, and reactions must be present to achieve the functionalities as implant materials.

5.2.2 Alkaline treatment

Surface modification can also be accomplished using alkaline treatment. In understanding the mechanism underlying the alkaline treatment, it is well known that titanium has a superior corrosion resistance due to its protective oxide layer that forms spontaneously when it comes into contact with oxygen in air. When titanium samples are immersed in alkaline solutions such as potassium hydroxide (KOH) or sodium hydroxide (NaOH), the alkaline solution attacks the protective oxide layer (TiO_2) and forms $HTiO_3$ compounds, as shown in Reaction (1). Following the dissolution of the TiO_2 layer, the bare surface of Ti reacted with the hydroxide ions to form a hydrogel layer composed of titanium oxide. Just after, the hydrated titanium oxide reacted with the hydroxide ions to form a sodium titanate hydrogel. The reaction is written as Reactions (2)−(5) [149,196,197]. Since the biocompatibility of titanium alloys is often measured in the capability of growing apatite in simulated body fluid (SBF), it is often described that alkali-treated Ti-based alloys with Ti—OH groups formed on the surface of sodium titanate hydrogel significantly enhanced the apatite growth, which plays an important role in osteoblastic differentiation during the early days of implantation. It has commonly been reported that alkali treatment of titanium-based alloys, followed by subsequent heat treatment, is capable of producing unique interconnected nano-pores on the surface, which are very beneficial as sites for nucleation and precipitation of Ca—P compounds. This porous

nanostructured surface improves oxygen exchange in cell metabolism and has long been recognized as the best structure for bone ingrowth and osseointegration [197,198]. Table 13 summarises some key findings concerning various Ti-based alloys that have been surface modified using alkaline treatment. According to the table, alkaline treatment is also not capable of standing on its own. Further treatment, usually involving the application of heat, is frequently required to alter the unstable phase of the sodium titanate hydrogel layer in order to increase the capability of inducing apatite deposition.

$$TiO_2+NaOH\rightarrow HTiO_3^-+Na^+ \quad (4)$$

$$Ti+3OH^-\rightarrow Ti(OH)_3^++4e \quad (5)$$

$$2Ti(OH)_3^++2e\rightarrow 2TiO_2\cdot H_2O+H_2\uparrow \quad (6)$$

$$Ti(OH)_3^++OH^-\rightleftharpoons Ti(OH)_4 \quad (7)$$

$$TiO_2\cdot nH_2O+OH^-\rightleftharpoons HTiO_3^-\cdot nH_2O \quad (8)$$

6 Challenges and future perspectives

A long-term application of implant in human body without bringing any undesirable effects is the most important concern including metallic implant such as Ti alloy. In the fabrication of Ti alloys, the processing parameters are always associated with challenges such as the control in grain size of various titanium phases, shape, orientation and distribution. Particularly, the characteristic of elastic modulus in Ti alloy that may lead to the stress shielding effect due to large mismatch with human bone is still the main concern and main challenge for Ti alloy development as an implant, although Ti alloys always have lower elastic modulus compared to other metallic biomaterials such as stainless steels and cobalt−chromium alloys [202]. For the future perspectives, a porous Ti-based alloys are considered to be a new invention, as the porous structure has been reported to promote the tissue

Table 13 Alkaline treatment techniques of various Ti-based alloys for implant application

Substrate	Applied treatment	Parameter of alkaline treatment	Significant findings related to biocompatibility	Ref.
cp-Ti	(1) AT + HT (2) IHT + AT + HT (3) IHT + AE + AT + HT	AT: 5 mol/L NaOH solution at 60 °C for 1 h; HT: 600 °C for 1 h IHT: 120 s at 380 V and 600 A; AE: mixed acid solution of H_2SO_4/HCl/H_2O= 1:1:2 (volume ratio) at 70 °C for 1 h	Apatite deposition on the surface is thicker for substrate that has been induction heated + acid etched + alkaline treatment + heat treatment	[199]
Ti−6Al−4V Ti−In−Nb−Ta	AT + HT	AT: 5.0 mol/L NaOH aqueous solution for 24 h; HT: 600 and 800 °C for 1 h	Alkaline and heat treatment performed on both alloys showed improved bioactive behavior, and Ti−In−Nb−Ta alloy had better bioactivity than that of Ti−6Al−4V upon immersion in simulated body fluid within the first 10 d; the intensity of the sodium titanate ($Na_2Ti_5O_{11}$ or $Na_2Ti_6O_{13}$) decreased when the heat treatment is carried out at 800 °C	[200]
Ti−24Nb−4Zr−8Sn	AT	5, 10 and 15 mol/L of NaOH solutions at room temperature for 48 h	The presence of $Na_2Ti_6O_{13}$ and $Na_2Ti_3O_7$ in XRD peaks suggested that there was a reaction took place between titanium oxides in MAO coating with NaOH during alkaline treatment; increasing concentration of the alkali caused an increase in the amount of sodium titanate phase; within only 7 d upon immersion in simulated body fluid, the amount of apatite deposits on the surface of alkaline treated sample in 15 mol/L NaOH is more than that of treated in 10 mol/L NaOH	[201]

IHT: Induction heat treatment; AT: Alkaline treatment; AE: Acidic treatment; HT: Heat treatment

ingrowth and firm-secure of an implant by controlling the degree of sintering [26]. In addition, the conventional powder metallurgy technique can be modified by improving the sintering way such as self-propagating high-temperature synthesis (SHS) [203].

Undeniably, another significant challenge in the development of Ti alloy implants is the issue of surface modification for the purpose of activating the surface to establish a bonding to the implantation sites. Surface modification methods include anodization, electrophoretic deposition, micro-arc oxidation, acid and alkaline treatment, sol-gel method, ion implantation, and many more. The research into their proclivity to generate a better bioactive surface layer should continue in order to make a new, excellent discovery. Clearly, advanced surface modification methods are highly concerned with creating better surface oxide nanotubes on Ti alloy with more advantages provided in the future.

7 Conclusions

Titanium and its alloys have been used as biomedical implants for decades. Long-term use of Ti alloys, such as commercially pure Ti and Ti−6Al−4V alloys, has been shown to have negative effects on human health. Therefore, numerous research efforts have been directed toward developing new Ti-based alloys that could eventually replace conventional implants, with the emphasis now on synthesizing Ti alloys with β-phase to reduce the elastic modulus to nearly that of bone. This review examines both conventional and advanced processing techniques, including powder metallurgy, selective laser melting, and electron beam melting. Each technique results in a different set of alloy properties, but the primary objective is for the Ti alloys to have sufficient properties to qualify as an implant material.

Since surface modification techniques are becoming increasingly important for inducing bioactivity characteristics on nearly inert Ti-based alloys, this review covers a wide range of techniques such as anodization, electrophoretic deposition, micro-arc deposition, acid and alkaline treatment. However, among the techniques available, anodization is the most promising method with numerous advantages in establishing nanostructured TiO_2 nanotubes on Ti substrate. Several anodization processes are reported on conventional Ti-based implants, such as cp-Ti and Ti−6Al−4V, according to a literature search. Both of these materials may no longer be used in the future because many other Ti-based alloys with much better properties in terms of bioactivity and close resemblance to human bone are currently being investigated. On the other hand, the scientific and systematic investigation carried out on anodization process of Ti-based alloys with the content of β-stabilizer is still quite limited to be reported over the literature, since this β-type Ti alloys actually display the best mimic to human bone in term of mechanical performance. Research on bulk properties of β-type Ti alloys shows a good resemblance to human bones in term of the elastic modulus, but as Ti itself is known to be nearly inert materials, effort towards imparting the bioactivity will be an important concern. Furthermore, research works that assess all of the critical properties of TiO_2 oxide nanotubes for that specific surface to be used in biological systems must be thoroughly investigated, as this aspect is not frequently reported in the literature.

Acknowledgments

This work was funded by the Malaysian Ministry of Higher Education under the Fundamental Research Grant Scheme (Project Code FRGS/1/2018/TK05/USM/01/5), and the first author is supported financially by a scholarship from Universiti Sains Malaysia (USM Fellowship).

References

[1] ZHANG Lai-chang, CHEN Liang-yu. A review on biomedical titanium alloys: Recent progress and prospect [J]. Advanced Engineering Materials, 2019, 21(4): 1801215.

[2] UHTHOFF H K, POITRAS P, BACKMAN D S. Internal plate fixation of fractures: Short history and recent developments [J]. Journal of Orthopaedic Science, 2006, 11(2): 118−126.

[3] GOMES C C, MOREIRA L M, SANTOS V J S V, RAMOS A S, LYON J P, SOARES C P, SANTOS F V. Assessment of the genetic risks of a metallic alloy used in medical implants [J]. Genetics and Molecular Biology, 2011, 34(1): 116−121.

[4] KAUR M, SINGH K. Review on titanium and titanium based alloys as biomaterials for orthopaedic applications [J]. Materials Science and Engineering C, 2019, 102: 844−862.

[5] BARRIOBERO-VILA P. Phase transformation kinetics during continuous heating of α+β and metastable β titanium alloys [M]. Vienna: Vienna University of Technology, 2014.

[6] BARRIOBERO-VILA P, REQUENA G, WARCHOMICKA F, STARK A, SCHELL N, BUSLAPS T. Phase transformation kinetics during continuous heating of a β-quenched Ti−10V−2Fe−3Al alloy [J]. Journal of Materials Science, 2015, 50(3): 1412−1426.

[7] BARRIOBERO-VILA P, REQUENA G, BUSLAPS T, ALFELD M, BOESENBERG U. Role of element partitioning on the α-β phase transformation kinetics of a bi-modal Ti−6Al−6V−2Sn alloy during continuous heating [J]. Journal of Alloys and Compounds, 2015, 626: 330−339.

[8] BARRIOBERO-VILA P, REQUENA G, SCHWARZ S, WARCHOMICKA F, BUSLAPS T. Influence of phase transformation kinetics on the formation of α in a β-quenched Ti−5Al−5Mo−5V−3Cr−1Zr alloy [J]. Acta Materialia, 2015, 95: 90−101.

[9] SHAH F A, TROBOS M, THOMSEN P, PALMQUIST A. Commercially pure titanium (cp-Ti) versus titanium alloy (Ti6Al4V) materials as bone anchored implants—Is one truly better than the other? [J]. Materials Science and Engineering C, 2016, 62: 960−966.

[10] BANERJEE D, WILLIAMS J C. Perspectives on titanium science and technology [J]. Acta Materialia, 2013, 61(3): 844−879.

[11] JUNG T K, SEMBOSHI S, MASAHASHI N, HANADA S. Mechanical properties and microstructures of β Ti−25Nb−11Sn ternary alloy for biomedical applications [J]. Materials Science and Engineering C, 2013, 33(3): 1629−1635.

[12] ABDEL-SALAM M, EL-HADAD S, KHALIFA W. Effects of microstructure and alloy composition on hydroxyapatite precipitation on alkaline treated α/β titanium alloys [J]. Materials Science and Engineering C, 2019, 104: 109974.

[13] FELLAH M, AISSANI L, SAMAD M A, IOST A, ZINE T M, MONTAGNE A, NOUVEAU C. Effect of replacing vanadium by niobium and iron on the tribological behavior of HIPed titanium alloys [J]. Acta Metallurgica Sinica (English Letters), 2017, 30(11): 1089−1099.

[14] MARSUMI Y, PRAMONO A W. Influence of niobium or molybdenum in titanium alloy for permanent implant application [J]. Advanced Materials Research, 2014, 900: 53−63.

[15] RHO J Y, TSUI T Y, PHARR G M. Elastic properties of human cortical and trabecular lamellar bone measured by nanoindentation [J]. Biomaterials, 1997, 18(20): 1325−1330.

[16] LI Yu-hua, YANG Chao, ZHAO Hai-dong, QU Sheng-guan, LI Xiao-qiang, LI Yuan-yuan. New developments of Ti-based alloys for biomedical applications [J]. Materials, 2014, 7(3): 1709−1800.

[17] BLACK J, HASTINGS G. Handbook of biomaterial properties [M]. Boston, MA: Springer, 1998.

[18] DEWIDAR M M, YOON H C, LIM J K. Mechanical properties of metals for biomedical applications using powder metallurgy process: A review [J]. Metals and Materials International, 2006, 12(3): 193−206.

[19] BAI Yan-jie, DENG Yi, ZHENG Yun-fei, LI Yong-liang, ZHANG Ran-ran, LV Ya-lin, ZHAO Qiang, WEI Shi-cheng. Characterization, corrosion behavior, cellular response and in vivo bone tissue compatibility of titanium−niobium alloy with low Young's modulus [J]. Materials Science and Engineering C, 2016, 59: 565−576.

[20] CHEN Qi-zhi, THOUAS G A. Metallic implant biomaterials [J]. Materials Science and Engineering R, 2015, 87: 1−57.

[21] MAVROS N, LARIMIAN T, ESQIVEL J, GUPTA R K, CONTIERI R, BORKAR T. Spark plasma sintering of low modulus titanium−niobium−tantalum−zirconium (TNTZ) alloy for biomedical applications [J]. Materials and Design, 2019, 183: 108163.

[22] YI Chang-bo, YUAN Yi-xiang, ZHANG Lei, JIANG Ye-hua, HE Zheng-yuan. Antibacterial Ti−35Nb−7Zr−xCu alloy with excellent mechanical properties generated with a spark plasma sintering method for biological applications [J]. Journal of Alloys and Compounds, 2021, 879: 160473.

[23] NIINOMI M, NARUSHIMA T, NAKAI M. Advances in metallic biomaterials – Processing and applications [M]. Berlin, Heidelberg: Springer, 2015.

[24] FROES F H. Titanium: physical metallurgy, processing and application [M]. United States of America: ASM International, 2015.

[25] LEYENS C, PETERS M. Titanium and titanium alloys: Fundamentals and applications [M]. Germany: John Wiley and Sons, 2003.

[26] BLAINE D C, BOSMAN H L, LAUBSCHER H H. Process models for press-and-sinter titanium [J]. Advanced Materials Research, 2014, 1019: 231−240.

[27] FROES F H. Powder metallurgy of titanium alloys in Advances in powder metallurgy [M]// Advances in Powder Metallurgy. Amsterdam: Elsevier, Woodhead Publishing, 2013: 202−240.

[28] KANG S J L. Sintering: densification, grain growth and microstructure [M]. Great Britain: Elsevier, 2005.

[29] KANG Li-mei, YANG Chao. A review on high-strength titanium alloys: Microstructure, strengthening, and properties [J]. Advanced Engineering Materials, 2019, 21(8): 1801359.

[30] YANG C, ZHU M D, LUO X, LIU L H, ZHANG W W, LONG Y, XIAO Z Y, FU Z Q, ZHANG L C, LAVERNIA E J. Influence of powder properties on densification mechanism during spark plasma sintering [J]. Scripta Materialia, 2017, 139: 96−99.

[31] LI X X, YANG C, CHEN T, FU Z Q, LI Y Y, IVASISHIN O M, LAVERNIA E J. Determination of atomic diffusion coefficient via isochronal spark plasma sintering [J]. Scripta Materialia, 2018, 151: 47−52.

[32] LI X X, YANG C, LU H Z, LUO X, LI Y Y, IVASISHIN O M. Correlation between atomic diffusivity and densification mechanism during spark plasma sintering of titanium alloy powders [J]. Journal of Alloys and Compounds, 2019, 787: 112−122.

[33] KARRE R, KODLI B K, RAJENDRAN A, NIVEDHITHA J, PATTANAYAK D K, AMEYAMA K, DEY S R. Comparative study on Ti−Nb binary alloys fabricated through spark plasma sintering and conventional P/M routes for biomedical application [J]. Materials Science and Engineering C, 2019, 94: 619−627.

[34] KONG Qing-quan, LAI Xin, AN Xu-guang, FENG Wei, LU Chao, WU Jiang, WU Chuan, WU Lian-ci, WANG Qing-yuan. Characterization and corrosion behavior of Ti−13Nb−13Zr alloy prepared by mechanical alloying and spark plasma sintering [J]. Materials Today Communications, 2020, 23: 101130.

[35] HUSSEIN M A, SURYANARAYANA C, AL-AQEELI N. Fabrication of nano-grained Ti−Nb−Zr biomaterials using spark plasma sintering [J]. Materials and Design, 2015, 87: 693−700.

[36] ZOU L M, YANG C, LONG Y, XIAO Z Y, LI Y Y. Fabrication of biomedical Ti−35Nb−7Zr−5Ta alloys by mechanical alloying and spark plasma sintering [J]. Powder Metallurgy, 2012, 55: 65−70.

[37] LI Y Y, ZOU L M, YANG C, LI Y H, LI L J. Ultrafine-grained Ti-based composites with high strength and low modulus fabricated by spark plasma sintering [J]. Materials Science and Engineering A, 2013, 560: 857−861.

[38] LI Y H, YANG C, WANG F, ZHAO H D, QU S G, LI X Q, ZHANG W W, LI Y Y. Biomedical TiNbZrTaSi alloys designed by d-electron alloy design theory [J]. Materials and Design, 2015, 85: 7−13.

[39] ZHANG Yi-wen, CHU Kang-jie, HE Shan, WANG Bi, ZHU Wei-wei, REN Fu-zeng. Fabrication of high strength, antibacterial and biocompatible Ti−5Mo−5Ag alloy for medical and surgical implant applications [J]. Materials Science and Engineering C, 2020, 106: 110165.

[40] ASL M S, DELBARI S A, AZADBEH M, NAMINI A S, MEHRABIAN M, NGUYEN V H, QUYET V L, SHOKOUHIMEHR M, MOHAMMADI M. Nanoindentational and conventional mechanical properties of spark plasma sintered Ti−Mo alloys [J]. Journal of Materials Research and Technology, 2020, 9: 10647−10658.

[41] YAMANOGLU R, GULSOY N, OLEVSKY E A, GULSOY H O. Production of porous Ti5Al2.5Fe alloy via pressureless spark plasma sintering [J]. Journal of Alloys and Compounds, 2016, 680: 654−658.

[42] QIAN M, YANG Y F, LUO S D, TANG H P. Pressureless sintering of titanium and titanium alloys: Sintering densification and solute homogenization [C]//Titanium Powder Metallurgy. United States of America: Butterworth-Heinemann, 2008: 201−218.

[43] BOLZONI L, RAYNOVA S, YANG F. Work hardening of microwave sintered blended elemental Ti alloys [J]. Journal of Alloys and Compounds, 2020, 838: 155559.

[44] COLOMBINI E, ROSA R, TROMBI L, ZADRA M, CASAGRANDE A, VERONESI P. High entropy alloys obtained by field assisted powder metallurgy route: SPS and microwave heating [J]. Materials Chemistry and Physics, 2018, 210: 78−86.

[45] IBRAHIM M K, HAMZAH E, SAUD S N, NAZIM E M, BAHADOR A. Parameter optimization of microwave sintering porous Ti−23%Nb shape memory alloys for biomedical applications [J]. Transactions of Nonferrous Metals Society of China, 2018, 28: 700−710.

[46] ZHENG Jing-pu, CHEN Liang-jian, CHEN Dai-yuan, SHAO Chun-sheng, YI Man-fei, ZHANG Bo. Effects of pore size and porosity of surface-modified porous titanium implants on bone tissue ingrowth [J]. Transactions of Nonferrous Metals Society of China, 2019, 29: 2534−2545.

[47] SINGHAL C, MURTAZA Q, PARVEJ. Microwave sintering of advanced composites materials: A review [J]. Materials Today: Proceedings, 2018, 5: 24287−24298.

[48] XU J L, TAO S C, BAO L Z, LUO J M, ZHENG Y F. Effects of Mo contents on the microstructure, properties and cytocompatibility of the microwave sintered porous Ti−Mo alloys [J]. Materials Science and Engineering C, 2019, 97: 156−165.

[49] TAO S C, XU J L, YUAN L, LUO J M, ZHENG Y F. Microstructure, mechanical properties and antibacterial properties of the microwave sintered porous Ti−3Cu alloys [J]. Journal of Alloys and Compounds, 2020, 812: 152142.

[50] PENG Qian, TANG Zhan-gui, WANG Yue-hong, PENG Zhi-wei. Mechanical performance and in-vitro biological behaviors of boronized Ti6Al4V/HA composites synthesized by microwave sintering [J]. Ceramics International, 2019, 45: 24684−24690.

[51] PRAKASH C, SINGH S, RAMAKRISHNA S, KRÖLCZYK G, LE C H. Microwave sintering of porous Ti−Nb−HA composite with high strength and enhanced bioactivity for implant applications [J]. Journal of Alloys and Compounds, 2020, 824: 153774.

[52] PRAKASH C, SINGH S, SHARMA S, SINGH J, SINGH G, MEHTA M, MITTAL M, KUMAR H. Fabrication of low elastic modulus $Ti_{50}Nb_{30}HA_{20}$ alloy by rapid microwave sintering technique for biomedical applications [J]. Materials Today: Proceedings, 2020, 21: 1713−1716.

[53] ZHURAVLEVA K, BÖNISCH M, SCUDINO S, CALIN M, SCHULTZ L, ECKERT J, GEBERT A. Phase transformations in ball-milled Ti−40Nb and Ti−45Nb powders upon quenching from the β-phase region [J]. Powder Technology, 2014, 253: 166−171.

[54] FARRAHNOOR A, ZUHAILAWATI H. Effects of hydroxyapatite addition on the bioactivity of Ti−Nb alloy matrix composite fabricated via powder metallurgy process [J]. Materials Today Communications, 2021, 27: 102209.

[55] DABHADE V V, RAMA MOHAN T R, RAMAKRISHNAN P. Synthesis of nanosized titanium powder by high energy milling [J]. Applied Surface Science, 2001, 182(3/4): 390−393.

[56] EL-ESKANDARANY S. Mechanical alloying: Nanotechnology, materials science and powder metallurgy [M]. United States of America: William Andrew Publishing, 2015.

[57] MOHAMAD RODZI S N H, ZUHAILAWATI H, DHINDAW B K. Mechanical and degradation behaviour of biodegradable magnesium−zinc/hydroxyapatite composite with different powder mixing techniques [J]. Journal of Magnesium and Alloys, 2019, 7(4): 566−576.

[58] FANG Z Z. Sintering of advanced materials: Fundamentals and processes [M]. United Kingdom: Woodhead Publishing Limited, 2010.

[59] CHEN Gang, CAO Peng, EDMONDS N. Porous NiTi alloys produced by press-and-sinter from Ni/Ti and Ni/TiH_2 mixtures [J]. Materials Science and Engineering A, 2013, 582: 117−125.

[60] RAO X, CHU C L, ZHENG Y Y. Phase composition, microstructure, and mechanical properties of porous Ti−Nb−Zr alloys prepared by a two-step foaming powder metallurgy method [J]. Journal of the Mechanical Behavior of Biomedical Materials, 2014, 34: 27−36.

[61] SONG Bo, ZHAO Xiao, LI Shuai, HAN Chang-jun, WEI Qing-song, WEN Shi-feng, LIU Jie, SHI Yu-sheng. Differences in microstructure and properties between selective laser melting and traditional manufacturing for fabrication of metal parts: A review [J]. Frontiers of Mechanical Engineering, 2015, 10(2): 111−125.

[62] LOWTHER M, LOUTH S, DAVEY A, HUSSAIN A, GINESTRA P, CARTER L, EISENSTEIN N, GROVER L, COX S. Clinical, industrial, and research perspectives on powder bed fusion additively manufactured metal implants [J]. Additive Manufacturing, 2019, 28: 565−584.

[63] CHILDERHOUSE T, JACKSON M. Near net shape manufacture of titanium alloy components from powder and wire: A review of state-of-the-art process routes [J]. Metals, 2019, 9(6): 689−706.

[64] WANG D W, ZHOU Y H, SHEN J, LIU Y, LI D F, ZHOU Q, SHA G, XU P, EBEL T, YAN M. Selective laser melting under the reactive atmosphere: A convenient and efficient approach to fabricate ultrahigh strength commercially pure titanium without sacrificing ductility [J]. Materials Science and Engineering A, 2019, 762: 138078.

[65] NA T W, KIM W R, YANG S M, KWON O, PARK J M, KIM G H, JUNG K H, LEE C W, PARK H K, KIM H G. Effect of laser power on oxygen and nitrogen concentration of commercially pure titanium manufactured by selective laser melting [J]. Materials Characterization, 2018, 143: 110−117.

[66] ATAEE A, LI Y C, BRANDT M, WEN C E. Ultrahigh-strength titanium gyroid scaffolds manufactured by selective laser melting (SLM) for bone implant applications [J]. Acta Materialia, 2018, 158: 354−368.

[67] LIU Y J, REN D C, LI S J, WANG H, ZHANG L C, SERCOMBE T B. Enhanced fatigue characteristics of a topology-optimized porous titanium structure produced by selective laser melting [J]. Additive Manufacturing, 2020, 32: 101060.

[68] WANG Qian, HAN Chang-jun, CHOMA T, WEI Qing-song, YAN Chun-ze, SONG Bo, SHI Yu-sheng. Effect of Nb content on microstructure, property and in vitro apatite-forming capability of Ti−Nb alloys fabricated via selective laser melting [J]. Materials and Design, 2017, 126: 268−277.

[69] SING S L, WIRIA F E, YEONG W Y. Selective laser melting of titanium alloy with 50 wt% tantalum: Effect of laser process parameters on part quality [J]. International Journal of Refractory Metals and Hard Materials, 2018, 77: 120−127.

[70] ZHAO Dan-lei, HAN Chang-jun, LI Yan, LI Jing-jing, ZHOU Kun, WEI Qing-song, LIU Jie, SHI Yu-sheng. Improvement on mechanical properties and corrosion resistance of titanium-tantalum alloys in-situ fabricated via selective laser melting [J]. Journal of Alloys and Compounds, 2019, 804: 288−298.

[71] YAN La-mei, YUAN You-wei, OUYANG Lin-jun, LI Hong, MIRZASADEGHI A, LI Li. Improved mechanical properties of the new Ti−15Ta−*x*Zr alloys fabricated by selective laser melting for biomedical application [J]. Journal of Alloys and Compounds, 2016, 688: 156−162.

[72] LI Yun-cang, DING Yun-fei, MUNIR K, LIN Jin-xing, BRANDT M, ATRENS A, XIAO Yin, KANWAR J R, WEN C E. Novel β-Ti35Zr28Nb alloy scaffolds manufactured using selective laser melting for bone implant applications [J]. Acta Biomaterialia, 2019, 87: 273−284.

[73] BARTOLOMEU F, BUCIUMEANU M, PINTO E, ALVES N, SILVA F S, CARVALHO O, MIRANDA G. Wear behavior of Ti6Al4V biomedical alloys processed by selective laser melting, hot pressing and conventional casting [J]. Transactions of Nonferrous Metals Society of China, 2017, 27(4): 829−838.

[74] LIANG Hui-xin, YANG You-wen, XIE De-qiao, LI Lan, MAO Ning, WANG Chang-jiang, TIAN Zong-jun, JIANG Qing, SHEN Li-da. Trabecular-like Ti−6Al−4V scaffolds for orthopedic: Fabrication by selective laser melting and in vitro biocompatibility [J]. Materials Science and Technology, 2019, 35(7): 1284−1297.

[75] MACPHERSON A, LI Xiao-peng, MCCORMICK P, REN Ling, YANG Ke, SERCOMBE T B. Antibacterial titanium produced using selective laser melting [J]. JOM, 2017, 69(12): 2719−2724.

[76] LUO J P, SUN J F, HUANG Y J, ZHANG J H, ZHANG Y D, ZHAO D P, YAN M. Low-modulus biomedical Ti−30Nb−5Ta−3Zr additively manufactured by selective laser melting and its biocompatibility [J]. Materials Science and Engineering C, 2019, 97: 275−284.

[77] LUO X, LIU L H, YANG C, LU H Z, MA H W, WANG Z, LI D D, ZHANG L C, LI Y Y. Overcoming the strength-ductility trade-off by tailoring grain-boundary metastable Si-containing phase in β-type titanium alloy [J]. Journal of Materials Science and Technology, 2021, 68: 112−123.

[78] CAI C, WU X, LIU W, ZHU W, CHEN H, QIU J C D, SUN C N, LIU J, WEI Q S, SHI Y S. Selective laser melting of near-α titanium alloy Ti−6Al−2Zr−1Mo−1V: Parameter optimization, heat treatment and mechanical performance [J]. Journal of Materials Science and Technology, 2020, 57: 51−64.

[79] LIU Y J, ZHANG Y S, ZHANG L C. Transformation-induced plasticity and high strength in beta titanium alloy manufactured by selective laser melting [J]. Materialia, 2019, 6: 100299.

[80] HAN Chang-jun, WANG Qian, SONG Bo, LI Wei, WEI Qing-song, WEN Shi-feng, LIU Jie, SHI Yu-sheng. Microstructure and property evolutions of titanium/ nano-hydroxyapatite composites in situ prepared by selective laser melting [J]. Journal of the Mechanical Behavior of Biomedical Materials, 2017, 71: 85−94.

[81] RACK H J, QAZI J I. Titanium alloys for biomedical applications [J]. Materials Science and Engineering C, 2006, 26(8): 1269−1277.

[82] SING S L, AN J, YEONG W Y, WIRIA F E. Laser and electron-beam powder-bed additive manufacturing of metallic implants: A review on processes, materials and designs [J]. Journal of Orthopaedic Research Society, 2016,

34(3): 369−385.

[83] LIU Y J, LI S J, WANG H L, HOU W T, HAO Y L, YANG R, SERCOMBE T B, ZHANG L C. Microstructure, defects and mechanical behavior of beta-type titanium porous structures manufactured by electron beam melting and selective laser melting [J]. Acta Materialia, 2016, 113: 56−67.

[84] LIU Y J, LI S J, HOU W T, WANG S G, HAO Y L, YANG R, SERCOMBE T B, ZHANG L C. Electron beam melted beta-type Ti−24Nb−4Zr−8Sn porous structures with high strength-to-modulus ratio [J]. Journal of Materials Science and Technology, 2016, 32(6): 505−508.

[85] ZHANG L C, KLEMM D, ECKERT J, HAO Y L, SERCOMBE T B. Manufacture by selective laser melting and mechanical behavior of a biomedical Ti−24Nb−4Zr−8Sn alloy [J]. Scripta Materialia, 2011, 65(11): 21−24.

[86] BALASUBRAMANIAN R, NAGUMOTHU R, PARFENOV E, VALIEV R. Development of nanostructured titanium implants for biomedical implants—A short review [J]. Materials Today: Proceedings, 2021, 46: 1195−1200.

[87] PRIYADARSHINI B, RAMYA S, SHINYJOY E, KAVITHA L, GOPI D, VIJAYALAKSHMI U. Structural, morphological and biological evaluations of cerium incorporated hydroxyapatite sol-gel coatings on Ti−6Al−4V for orthopaedic applications [J]. Journal of Materials Research and Technology, 2021, 12: 1319−1338.

[88] NIINOMI M, NAKAI M, HIEDA J. Development of new metallic alloys for biomedical applications [J]. Acta Biomaterialia, 2012, 8(11): 3888−3903.

[89] YANG Dong-hua, GUO Zhi-meng, SHAO Hui-ping, LIU Xiao-ting, JI Ye. Mechanical properties of porous Ti−Mo and Ti−Nb alloys for biomedical application by gelcasting [J]. Procedia Engineering, 2012, 36: 160−167.

[90] GUO Shun, MENG Qing-kun, ZHAO Xin-qing, WEI Qiu-ming, XU Hui-bin. Design and fabrication of a metastable β-type titanium alloy with ultralow elastic modulus and high strength [J]. Scientific Reports, 2015, 5: 14688.

[91] HAN M K, KIM J Y, HWANG M J, SONG H J, PARK Y J. Effect of Nb on the microstructure, mechanical properties, corrosion behaviour, and cytotoxicity of Ti−Nb alloys [J]. Materials, 2015, 8(9): 5986−6003.

[92] KIM S E, JEONG H W, HYUN Y T, LEE Y T, JUNG C H, KIM S K, SONG J S, LEE J H. Elastic modulus and in-vitro biocompatibility of Ti−xNb and Ti−xTa alloys [J]. Metals and Materials International, 2007, 13(2): 145−149.

[93] FIKENI L, ANNAN K A, MUTOMBO K, MACHAKA R. Effect of Nb content on the microstructure and mechanical properties of binary Ti−Nb alloys [J]. Materials Today: Proceedings, 2020, 38: 913−917.

[94] CHEN Yun-hui, HAN Ping-ping, DEHGHAN-MANSHADI A, KENT D, EHTEMAM-HAGHIGHI S, JOWERS C, BERMINGHAM M, LI Tong, COOPER-WHITE J, DARGUSCH M S. Sintering and biocompatibility of blended elemental Ti−xNb alloys [J]. Journal of the Mechanical Behavior of Biomedical Materials, 2020, 104: 103691.

[95] CHANG L L, WANG Y D, REN Y. In-situ of stress-induced martensitic transformation in Ti−Nb binary alloys with low Young's modulus [J]. Materials Science and Engineering A, 2016, 651: 442−448.

[96] FARRAH NOOR A, ZUHAILAWATI H. A brief review on the properties of titanium as a metallic biomaterials [J]. International Journal of Electroactive Materials, 2020, 8: 63−67.

[97] BAI Yan-jie, DENG Yi, ZHENG Yun-fei, LI Yong-liang, ZHANG Ran-ran, LV Ya-lin, ZHAO Qiang, WEI Shi-cheng. Characterization, corrosion behaviour, cellular response and in vivo bone tissue compatibility of titanium-niobium alloy with low Young's modulus [J]. Materials Science and Engineering C, 2016, 59: 565−576.

[98] ZHOU Y L, NIINOMI M. Microstructures and mechanical properties of Ti−50mass%Ta alloy for biomedical applications [J]. Journal of Alloys and Compounds, 2008, 466(1/2): 535−542.

[99] XIE Fang-xia, HE Xin-bo, LU Xin, CAO Shun-li, QU Xuan-hui. Preparation and properties of porous Ti−10Mo alloy by selective laser sintering [J]. Materials Science and Engineering C, 2013, 33(3): 1085−1090.

[100] ZHAO Xing-feng, NIINOMI M, NAKAI M, HIEDA J. Beta type Ti−Mo alloys with changeable Young's modulus for spinal fixation applications [J]. Acta Biomaterialia, 2012, 8(5): 1990−1997.

[101] ZHAO X F, NIINOMI M, NAKAI M, HIEDA J, ISHIMOTO T, NAKANO T. Optimization of Cr content of metastable β-type Ti−Cr alloys with changeable Young's modulus for spinal fixation applications [J]. Acta Biomaterialia, 2012, 8(6): 2392−2400.

[102] EHTEMAM-HAGHIGHI S, LIU Yu-jing, CAO Guang-hui, ZHANG Lai-chang. Influence of Nb on the $\beta\rightarrow\alpha''$ martensitic phase transformation and properties of the newly designed Ti−Fe−Nb alloys [J]. Materials Science and Engineering C, 2016, 60: 503−510.

[103] KURODA D, KAWASAKI H, YAMAMOTO A, HIROMOTO S, HANAWA T. Mechanical properties and microstructures of new Ti−Fe−Ta and Ti−Fe−Ta−Zr system alloys [J]. Materials Science and Engineering C, 2005, 25(3): 312−320.

[104] EHTEMAM-HAGHIGHI S, CAO Guang-hui, ZHANG Lai-chang. Nanoindentation study of mechanical properties of Ti based alloys with Fe and Ta additions [J]. Journal of Alloys and Compounds, 2017, 692: 892−897.

[105] HO W F, WU S C, HSU S K, LI Y C, HSU H C. Effects of molybdenum content on the structure and mechanical properties of as-cast Ti−10Zr-based alloys for biomedical applications [J]. Materials Science and Engineering C, 2012, 32(3): 517−522.

[106] JAWED S F, RABADIA C D, LIU Y J, WANG L Q, LI Y H, ZHANG X H, ZHANG L C. Mechanical characterization and deformation behavior of β-stabilized Ti−Nb−Sn−Cr alloys [J]. Journal of Alloys and Compounds, 2019, 792: 684−693.

[107] WENG Wei-jie, BIESIEKIERSKI A, LIN Ji-xing, OZAN S, LI Yun-cang, WEN C E. Development of beta-type Ti−Nb−Zr−Mo alloys for orthopedic applications [J]. Applied Materials Today, 2021, 22: 100968.

[108] DAI S J, WANG Y, CHEN F, YU X Q, ZHANG Y F. Influence of Zr content on microstructure and mechanical properties of implant Ti−35Nb−4Sn−6Mo−*x*Zr alloys [J]. Transactions of Nonferrous Metals Society of China, 2013, 23(5): 1299−1303.

[109] SASIKUMAR Y, INDIRA K, RAJENDRAN N. Surface modification methods for titanium and its alloys and their corrosion behaviour in biological environment: A review [J]. Journal of Bio- and Tribo-Corrosion, 2019, 5(3): 1−25.

[110] ASRI R I M, HARUN W S W, SAMYKANO M, LAH N A C, GHANI S A C, TARLOCHAN F, RAZA M R. Corrosion and surface modification on biocompatible metals: A review [J]. Materials Science and Engineering C, 2017, 77: 1261−1274.

[111] MOCQUOT C, ATTIK N, PRADELLE-PLASSE N, GROSGOGEAT B, COLON P. Bioactivity assessment of bioactive glasses for dental applications: A critical review [J]. Dental Materials, 2020, 36(9): 1116−1143.

[112] TAN A W, PINGGUAN-MURPHY B, AHMAD R, AKBAR S A. Review of titania nanotubes: Fabrication and cellular response [J]. Ceramics International, 2012, 38(6): 4421−4435.

[113] AJEEL S A, ALI A M, KARM Z. Titanium oxide nanotube arrays used in implant materials [J]. UPB Scientific Bulletin Series B: Chemistry and Materials Science, 2014, 76: 95−104.

[114] REGONINI D, BOWEN C R, JAROENWORALUCK A, STEVENS R. A review of growth mechanism, structure and crystallinity of anodized TiO_2 nanotubes [J]. Materials Science and Engineering R, 2013, 74: 377−406.

[115] KULKARNI M, MAZARE A, GONGADZE E, PERUTKOVA Š, KRALJ-IGLIČ V, MILOŠEV I, SCHMUKI P, IGLIČ A, MOZETIČ M. Titanium nanostructures for biomedical applications [J]. Nanotechnology, 2015, 26(6): 062002.

[116] LIANG Yan-qin, YANG Xian-jin, CUI Zhen-duo, ZHU Sheng-li. Effect of TiO_2 nanotube morphology on the formation of apatite layer in simulated body fluid [J]. Current Nanoscience, 2010, 6(3): 256−261.

[117] BAI Y, PARK I S, PARK H H, LEE M H, BAE T S, DUNCAN W, SWAIN M. The effect of annealing temperatures on surface properties, hydroxyapatite growth and cell behaviors of TiO_2 nanotubes [J]. Surface and Interface Analysis, 2011, 43(6): 998−1005.

[118] CHERNOZEM R V, SURMENEVA M A, SURMENEV R A. Influence of anodization time and voltage on the parameters of TiO_2 nanotubes [J]. IOP Conference Series Materials Science and Engineering, 2016, 116: 012025.

[119] INDIRA K, MUDALI U K, NISHIMURA T, RAJENDRAN N. A review on TiO_2 nanotubes: Influence of anodization parameters, formation mechanism, properties, corrosion behaviour and biomedical applications [J]. Journal of Bio- and Tribo-Corrosion, 2015, 1(4): 1−22.

[120] SREEKANTAN S, SAHARUDIN K A, WEI L C. Formation of TiO_2 nanotubes via anodization and potential applications for photocatalysts, biomedical materials, and photoelectrochemical cell [J]. IOP Conference Series: Materials Science and Engineering, 2011, 21: 012002.

[121] ELIAS C N, FERNANDES D J, de SOUZA F M, MONTEIRO E D S, de BIASI R S. Mechanical and clinical properties of titanium and titanium-based alloys (Ti G2, Ti G4 cold worked nanostructured and Ti G5) for biomedical applications [J]. Journal of Materials Research and Technology, 2019, 8(1): 1060−1069.

[122] PONSONNET L, REYBIER K, JAFFREZIC N, COMTE V, LAGNEAU C, LISSAC M, MARTELET C. Relationship between surface properties (roughness, wettability) of titanium and titanium alloys and cell behavior [J]. Materials Science and Engineering C, 2003, 23(4): 551−560.

[123] ESCADA A L, NAKAZATO R Z, CLARO A P R A. Influence of anodization parameters in the TiO_2 nanotubes formation on Ti−7.5Mo alloy surface for biomedical application [J]. Materials Research, 2017, 20(5): 1282−1290.

[124] WANG Qing-ge, ZHOU Peng, LIU Shi-feng, ATTARILAR S, MA R L W, ZHONG Yin-sheng, WANG Li-qiang. Multi-scale surface treatments of titanium implants for rapid osseointegration: A review [J]. Nanomaterials, 2020, 10(6): 1244.

[125] BRAMMER K S, OH S, COBB C J, BJURSTEN L M, van der HEYDE H, JIN S. Improved bone-forming functionality on diameter-controlled TiO_2 nanotube surface [J]. Acta Biomaterialia, 2009, 5(8): 3215−3223.

[126] LIU Guo-hua, DU Kang, WANG Kai-ying. Surface wettability of TiO_2 nanotube arrays prepared by electrochemical anodization [J]. Applied Surface Science, 2016, 388: 313−320.

[127] ZHAO Ming-hui, LI Ji-dong, LI Yu-bao, WANG Jian, ZUO Yi, JIANG Jia-xing, WANG Hua-nan. Gradient control of the adhesive force between Ti/TiO_2 nanotubular arrays fabricated by anodization [J]. Scientific Reports, 2014, 4: 7178.

[128] LONG Dong-ping, XUE Jian-rong, YAN Zhi-xin. Study on high order TiO_2 nanotube arrays and the mechanical properties [J]. Advanced Materials Research, 2013, 842: 247−251.

[129] DECHA-UMPHAI D, CHUNATE H T, PHETRATTANARANGSI T, BOONCHUDUANG T, CHOOSRI M, PUNCREOBUTR C, LOHWONGWATANA B, KHAMWANNAH J. Effects of post-processing on microstructure and adhesion strength of TiO_2 nanotubes on 3D-printed Ti−6Al−4V alloy [J]. Surface and Coatings Technology, 2021, 421: 127431.

[130] SARRAF M, RAZAK A, CRUM R, GÁMEZ C, RAMIREZ B, ABU KASIM N H, NASIRI-TABRIZI B, GUPTA V, SUKIMAN N L, BASIRUN W J. Adhesion measurement of highly-ordered TiO_2 nanotubes on Ti−6Al−4V alloy [J]. Processing and Application of Ceramics, 2017, 11(4): 311−321.

[131] PEREIRA B L, BEILNER G, LEPIENSKI C M, de SOUZA G B, KUROMOTO N K, SZAMEITAT E S, PENG A N S, LEE J Y, CLARO A P R A, NUGENT M J D. Scratch-resistant and well-adhered nanotube arrays produced via anodizing process on β-titanium alloy [J]. Materials Today Communications, 2021, 26: 101947.

[132] CRAWFORD G A, CHAWLA N, DAS K, BOSE S, BANDYOPADHYAY A. Microstructure and deformation

behavior of biocompatible TiO_2 nanotubes on titanium substrate [J]. Acta Biomaterialia, 2007, 3(3): 359−367.

[133] BORRA R C, LOTUFO M A, GAGIOTI S M, de MESQUITA BARROS F, ANDRADE P M. A simple method to measure cell viability in proliferation and cytotoxicity assays [J]. Brazilian Oral Research, 2009, 23(3): 255−262.

[134] MOHAN L, KAR S, HATTORI R, ISHII-TESHIMA M, BERA P, ROY S, SANTRA T S, SHIBATA T, NAGAI M. Can titanium oxide nanotubes facilitate intracellular delivery by laser-assisted photoporation? [J]. Applied Surface Science, 2021, 543: 148815.

[135] MOHAMED M S, TORABI A, PAULOSE M, KUMAR D S, VARGHESE O K. Anodically grown titania nanotube induced cytotoxicity has genotoxic origins [J]. Scientific Reports, 2017, 7: 41844.

[136] ALVES CLARO A P R, KONATU R T, ESCADAA L D A, de SOUZA NUNES M C, MAURER-MORELLI C V, DIAS-NETIPANYJ M F, POPAT K C, MANTOVANI D. Incorporation of silver nanoparticles on Ti7.5Mo alloy surface containing TiO_2 nanotubes arrays for promoting antibacterial coating—In vitro and in vivo study [J]. Applied Surface Science, 2018, 455: 780−788.

[137] CHERNOZEM R V, SURMENEVA M A, IGNATOV V P, PELTEK O O, GONCHARENKO A A, MUSLIMOV A R, TIMIN A S, TYURIN A I, IVANOV Y F, GRANDINI C R, SURMENEV R A. Comprehensive characterization of titania nanotubes fabricated on Ti−Nb alloys: Surface topography, structure, physico mechanical behavior and a cell culture assay [J]. ACS Biomaterials Science and Engineering, 2020, 6(3): 1487−1499.

[138] TAIPINA M O, de MELLO M G, TAMBORLIN L, PEREIRA K D, LUCHESSI A D, CREMASCO A, CARAM R. A novel Ag doping Ti alloys route: Formation and antibacterial effect of the TiO_2 nanotubes [J]. Materials Chemistry and Physics, 2021, 261: 124192.

[139] MICHALKOVA H, SKUBALOVA Z, SOPHA H, STRMISKA V, TESAROVA B, DOSTALOVA S, SVEC P, HROMADKO L, MOTOLA M, MACAK J M, ADAM V, HEGER Z. Complex cytotoxicity mechanism of bundles formed from self-organised 1-D anodic TiO_2 nanotubes layers [J]. Journal of Hazardous Materials, 2020, 388: 122054.

[140] LUZ A R, SANTOS L S, LEPIENSKI C M, KURODA P B, KUROMOTO N K. Characterization of the morphology, structure and wettability of phase dependent lamellar and nanotube oxides on anodized Ti−10Nb alloy [J]. Applied Surface Science, 2018, 448: 30−40.

[141] JAROSZ M, GRUDZIEŃ J, KAPUSTA-KOŁODZIEJ J, CHUDECKA A, SOŁTYS M, SULKA G D. Anodization of titanium alloys for biomedical applications [M]//Nanostructured Anodic Metal Oxides. Amsterdam: Elsevier, 2020: 211−275.

[142] GROTBERG J, HAMLEKHAN A, BUTT A, PATEL S, ROYHMAN D, SHOKUHFAR T, SUKOTJO C, TAKOUDIS C, MATHEW M T. Thermally oxidized titania nanotubes enhance the corrosion resistance of Ti−6Al−4V [J]. Materials Science and Engineering C, 2016, 59: 677−689.

[143] KONATU R T, DOMINGUES D D, ESCADA A L A, CHAVES J A M, NETIPANYJ M F D, NAKAZATO R Z, POPAT K C, GRANDINI C R, ALVES CLARO A P R. Synthesis and characterization of self-organized TiO_2 nanotubes grown on Ti−15Zr alloy surface to enhance cell response [J]. Surfaces and Interfaces, 2021, 26: 101439.

[144] HAZAN R, SREEKANTAN S, MYDIN R B S M N. Corrosion study on different phases of TiO_2 nanotubes in human body fluid environment [J]. AIP Conference Proceedings, 2019, 2068(1): 020013.

[145] OLIVEIRA N T C, VERDÉRIO J F, BOLFARINI C. Obtaining self-organized nanotubes on biomedical Ti−Mo alloys [J]. Electrochemistry Communications, 2013, 35: 139−141.

[146] VASILESCU C, DROB S I, NEACSU E I, MIRZA ROSCA J C. Surface analysis and corrosion resistance of a new titanium base alloy in simulated body fluids [J]. Corrosion Science, 2012, 65: 431−440.

[147] PISHBIN F, CORDERO-ARIAS L, CABANAS-POLO S, BOCCACCINI A R. Bioactive polymer-calcium phosphate composite coatings by electrophoretic deposition [M]//Surface Coating and Modification of Metallic Biomaterials. Amsterdam: Elsevier, 2015: 359−377.

[148] ALIPAL J, MOHD PUÁD N A S, NAYAN N H M, SAHARI N, ABDULLAH H Z, IDRIS M I, LEE T C. An updated review on surface functionalisation of titanium and its alloys for implants applications [J]. Materials Today: Proceedings, 2021, 42: 270−282.

[149] LIU Xuan-yong, CHU P K, DING Chuan-xian. Surface modification of titanium, titanium alloys, and related materials for biomedical applications [J]. Materials Science and Engineering R, 2004, 47(3/4): 49−121.

[150] KULKARNI M, MAZARE A, SCHMUKI P, IGLIČ A. Biomaterial surface modification of titanium and titanium alloys for medical applications [M]//Nanomedicine. New York: Springer Heidelberg, 2014.

[151] SANKARA NARAYANAN T S N, KIM J, PARK H W. Fabrication and synthesis of uniform TiO_2 nanoporous and nanotubular structures on dual-phase Ti−6Al−4V alloy using electron-beam irradiation [J]. Materials Chemistry and Physics, 2020, 242: 122549.

[152] Anodization of Ti and its alloys. https://www.sciencedirect.com/search?qs=anodization%20of%20Ti%20and%20its%20alloys&years=2012%2C2013%2C2014%2C2015%2C2016%2C2017%2C2018%2C2019%2C2020%2C2021%2C2022&lastSelectedFacet=years. Accessed on 29/9/2021.

[153] MACAK J M, TSUCHIYA H, GHICOV A, YASUDA K, HAHN R, BAUER S, SCHMUKI P. TiO_2 nanotubes: Self-organized electrochemical formation, properties and applications [J]. Current Opinion in Solid State and Materials Science, 2007, 11(1/2): 3−18.

[154] ALIPAL J, LEE T C, KOSHY P, ABDULLAH H Z, IDRIS M I. Evolution of anodised titanium for implant applications [J]. Heliyon, 2021, 7(7): e07408.

[155] BERGER S, ALBU S P, SCHMIDT-STEIN F, HILDEBRAND H, SCHMUKI P, HAMMOND J S, PAUL D F, REICHLMAIER S. The origin for tubular growth of TiO_2 nanotubes: A fluoride rich layer between tube-walls [J].

Surface Science, 2011, 605(19/20): L57−L60.
[156] LUZ A R, DE SOUZA G B, LEPIENSKI C M, SIQUEIRA C J M, KUROMOTO N K. Tribological properties of nanotubes grown on Ti−35Nb alloy by anodization [J]. Thin Solid Films, 2018, 660: 529−537.
[157] FERREIRA E A, ROCHA-FILHO R C, BIAGGIO S R, BOCCHI N. Corrosion resistance of the Ti−50Zr at.% alloy after anodization in different acidic electrolytes [J]. Corrosion Science, 2010, 52(12): 4058−4063.
[158] LUZ A R, LEPIENSKI C M, HENKE S L, GRANDINI C R, KUROMOTO N K. Effect of microstructure on the nanotube growth by anodic oxidation on Ti−10Nb alloy [J]. Materials Research Express, 2017, 4(7): 076408.
[159] JANG S H, CHOE H C, KO Y M, BRANTLEY W A. Electrochemical characteristics of nanotubes formed on Ti−Nb alloys [J]. Thin Solid Films, 2009, 517(17): 5038−5043.
[160] JHA H, HAHN R, SCHMUKI P. Ultrafast oxide nanotube formation on TiNb, TiZr and TiTa alloys by rapid breakdown anodization [J]. Electrochimica Acta, 2010, 55(28): 8883−8887.
[161] FENG X J, MACAK J M, SCHMUKI P. Flexible self-organization of two size-scales oxide nanotubes on Ti45Nb alloy [J]. Electrochemistry Communications, 2007, 9(9): 2403−2407.
[162] SUN Yan, YAN Kang-ping. Effect of anodization voltage on performance of TiO_2 nanotube arrays for hydrogen generation in a two-compartment photoelectrochemical cell [J]. International Journal of Hydrogen Energy, 2014, 39(22): 11368−11375.
[163] SU Zi-xue, ZHOU Wu-zong. Pore diameter control in anodic titanium and aluminium oxides [J]. J Mater Chem, Chemistry, 2011, 21(2): 357−362.
[164] PARK J, BAUER S, von der MARK K, SCHMUKI P. Nanosize and vitality: TiO_2 nanotube diameter directs cell fate [J]. Nano Letters, 2007, 7(6): 1686−1691.
[165] CHATTERJEE S, GINZBERG M, GERSTEN B. Effect of anodization conditions on the synthesis of TiO_2 nanopores [J]. MRS Proceedings, 2006, 951: 951-E09.
[166] MOHAN L, DENNIS C, PADMAPRIYA N, ANANDAN C, RAJENDRAN N. Effect of electrolyte temperature and anodization time on formation of TiO_2 nanotubes for biomedical applications [J]. Materials Today Communications, 2020, 23: 101103.
[167] ZHOU Qin-yi, TIAN Meng-meng, YING Zong-rong, DAN Yu-xin, TANG Feng-rui, ZHANG Jian-peng, ZHU Jun-wu, ZHU Xu-fei. Dense films formed during Ti anodization in NH_4F electrolyte: Evidence against the field-assisted dissolution reactions of fluoride ions [J]. Electrochemistry Communications, 2020, 111: 106663.
[168] KACZMAREK A, KLEKIEL T, KRASICKA-CYDZIK E. Fluoride concentration effect on the anodic growth of self-aligned oxide nanotube array on Ti_6Al_7Nb alloy [J]. Surface and Interface Analysis, 2010, 42(6/7): 510−514.
[169] NGUYEN Q A, BHARGAVA Y V, DEVINE T M. Titania nanotube formation in chloride and bromide containing electrolytes [J]. Electrochemistry Communications, 2008, 10(3): 471−475.
[170] HAHN R, MACAK J M, SCHMUKI P. Rapid anodic growth of TiO_2 and WO_3 nanotubes in fluoride free electrolytes [J]. Electrochemistry Communications, 2007, 9(5): 947−952.
[171] SREEKANTAN S, LOCKMAN Z, HAZAN R, TASBIHI M, TONG L K, MOHAMED A R. Influence of electrolyte pH on TiO_2 nanotube formation by Ti anodization [J]. Journal of Alloys and Compounds, 2009, 485(1/2): 478−483.
[172] TSUCHIYA H, MACAK J M, MÜLLER L, KUNZE J, MÜLLER F, GREIL P, VIRTANEN S, SCHMUKI P. Hydroxyapatite growth on anodic TiO_2 nanotubes [J]. Journal of Biomedical Materials Research A, 2006, 77A(3): 534−541.
[173] WANG Gui-fang, LI Jin-hua, LV Kai-ge, ZHANG Wen-jie, DING Xun, YANG Guang-zheng, LIU Xuan-yong, JIANG Xin-quan. Surface thermal oxidation on titanium implants to enhance osteogenic activity and in vivo osseointegration [J]. Scientific Reports, 2016, 6: 31769.
[174] LI Qing-biao, YANG Wen-bin, LIU Can-can, WANG Dao-ai, LIANG Jun. Correlations between the growth mechanism and properties of micro-arc oxidation coatings on titanium alloys: Effect of electrolytes [J]. Surface and Coatings Technology, 2017, 316: 162−170.
[175] WANG Dong-dong, LIU Xin-tong, WANG Yan, ZHANG Qing, LI Da-long, LIU Xin-ru, SU Hao, ZHANG Yu-huan, YU Sheng-xue, SHEN De-jiu. Role of the electrolyte composition in establishing plasma discharges and coating growth process during a micro-arc oxidation [J]. Surface and Coatings Technology, 2020, 402: 126349.
[176] FATTAH-ALHOSSEINI A, BABAEI K, MOLAEI M. Plasma electrolytic oxidation (PEO) treatment of zinc and its alloys: A review [J]. Surfaces and Interfaces, 2020, 18: 100441.
[177] WANG Ya-ping, ZHAO Shu-yue, LI Guo-qiang, ZHANG Shu-fang, ZHAO Rong-fang, DONG An-jie, ZHANG Rong-fa. Preparation and in vitro antibacterial properties of anodic coatings co-doped with Cu, Zn, and P on a Ti−6Al−4V alloy [J]. Materials Chemistry and Physics, 2020, 241: 122360.
[178] YIGIT O, DIKICI B, OZDEMIR N, ARSLAN E. Plasma electrolytic oxidation of Ti−6Al−4V alloys in *n*HA/GNS containing electrolytes for biomedical applications: The combined effect of the deposition frequency and GNS weight percentage [J]. Surface and Coatings Technology, 2021, 415: 127139.
[179] ZHOU Lan, LÜ Guo-hua, MAO Fei-fei, YANG Si-ze. Preparation of biomedical Ag incorporated hydroxyapatite/ titania coatings on Ti6Al4V alloy by plasma electrolytic oxidation [J]. Chinese Physics B, 2014, 23(3): 035205.
[180] TANASE C E, GOLOZAR M, BEST S M, BROOKS R A. Cell response to plasma electrolytic oxidation surface-modified low-modulus β-type titanium alloys [J]. Colloids and Surfaces B: Biointerfaces, 2019, 176: 176−184.
[181] KAZEK-KĘSIK A, DERCZ G, KALEMBA I, SUCHANEK K, KUKHARENKO A I, KOROTIN D M, MICHALSKA J, KRZĄKAŁA A, PIOTROWSKI J, KURMAEV E Z, CHOLAKH S O, SIMKA W. Surface characterization of Ti−15Mo alloy modified by a PEO process in various suspensions [J]. Materials Science and Engineering C, 2014,

39: 259−272.

[182] JING Wen-sen, ZHANG Ming-hua, JIN Lei, ZHAO Jian, GAO Qing, REN Min, FAN Qing-yu. Assessment of osteoinduction using a porous hydroxyapatite coating prepared by micro-arc oxidation on a new titanium alloy [J]. International Journal of Surgery, 2015, 24: 51−56.

[183] ZHAI Da-jun, FENG Ke-qin. Preparation of micro/nano-structured ceramic coatings on Ti6Al4V alloy by plasma electrolytic oxidation process [J]. Transactions of Nonferrous Metals Society of China, 2019, 29(12): 2546−2555.

[184] PESODE P A, BARVE S B. Recent advances on the antibacterial coating on titanium implant by micro-arc oxidation process [J]. Materials Today: Proceedings, 2021, 47: 5652−5662.

[185] ALIOFKHAZRAEI M, MACDONALD D D, MATYKINA E, PARFENOV E V, EGORKIN V S, CURRAN J A, TROUGHTON S C, SINEBRYUKHOV S L, GNEDENKOV S V, LAMPKE T, SIMCHEN F, NABAVI H F. Review of plasma electrolytic oxidation of titanium substrates: Mechanism, properties, applications and limitations [J]. Applied Surface Science Advances, 2021, 5: 100121.

[186] MEHNATH S, ARJAMA M, RAJAN M, PREMKUMAR K, KARTHIKEYAN K, JEYARAJ M. Mineralization of bioactive marine sponge and electrophoretic deposition on Ti−6Al−4V implant for osteointegration [J]. Surface and Coatings Technology, 2020, 392: 125727.

[187] MOSKALEWICZ T, ZYCH A, KRUK A, KOPIA A, ZIMOWSKI S, SITARZ M, CIENIEK Ł. Electrophoretic deposition and microstructure development of Si_3N_4/ polyetheretherketone coatings on titanium alloy [J]. Surface and Coatings Technology, 2018, 350: 633−647.

[188] KHANMOHAMMADI S, OJAGHI ILKHCHI M, KHALIL-ALLAFI J. Electrophoretic deposition and characterization of bioglass-whisker hydroxyapatite nanocomposite coatings on titanium substrate [J]. Surface and Coatings Technology, 2019, 378: 124949.

[189] FARNOUSH H, ALD1Ç G, ÇIMENOĞLU H. Functionally graded HA-TiO_2 nanostructured composite coating on Ti−6Al−4V substrate via electrophoretic deposition [J]. Surface and Coatings Technology, 2015, 265: 7−15.

[190] HADIDI M, BIGHAM A, SAEBNOORI E, HASSANZADEH-TABRIZI S A, RAHMATI S, ALIZADEH Z M, NASIRIAN V, RAFIENIA M. Electrophoretic-deposited hydroxyapatite−copper nano-composite as an antibacterial coating for biomedical applications [J]. Surface and Coatings Technology, 2017, 321: 171−179.

[191] KRUK A, ZIMOWSKI S, ŁUKASZCZYK A, CIENIEK Ł, MOSKALEWICZ T. The influence of heat treatment on the microstructure, surface topography and selected properties of PEEK coatings electrophoretically deposited on the Ti−6Al−4V alloy [J]. Progress in Organic Coatings, 2019, 133: 180−190.

[192] VLCAK P, FOJT J, KOLLER J, DRAHOKOUPIL J, SMOLA V. Surface pre-treatments of Ti−Nb−Zr−Ta beta titanium alloy: The effect of chemical, electrochemical and ion sputter etching on morphology, residual stress, corrosion stability and the MG-63 cell response [J]. Results in Physics, 2021, 28: 104613.

[193] TAKEUCHI M, ABE Y, YOSHIDA Y, NAKAYAMA Y, OKAZAKI M, AKAGAWA Y. Acid pretreatment of titanium implants [J]. Biomaterials, 2003, 24(10): 1821−1827.

[194] ESCOBAR CLAROS C A, CONTRI CAMPANELLI L, MOREIRA JORGE A Jr, LEPRÊTRE J C, BOLFARINI C, ROCHE V. Corrosion behavior of biomedical β-titanium alloys with the surface-modified by chemical etching and electrochemical methods [J]. Corrosion Science, 2021, 188: 109544.

[195] ZHAN Xin-xin, LI Shu-jun, CUI Yun-tao, TAO An-qi, WANG Cheng-cheng, LI Hua-zhi, ZHANG Lin-lin, YU Han-rong, JIANG Jiu-hui, LI Cui-ying. Comparison of the osteoblastic activity of low elastic modulus Ti−24Nb−4Zr−8Sn alloy and pure titanium modified by physical and chemical methods [J]. Materials Science and Engineering C, 2020, 113: 111018.

[196] FAURE J, BALAMURUGAN A, BENHAYOUNE H, TORRES P, BALOSSIER G, FERREIRA J M F. Morphological and chemical characterization of biomimetic bone like apatite formation on alkali treated Ti_6Al_4V titanium alloy [J]. Materials Science and Engineering C, 2009, 29(4): 1252−1257.

[197] CHEN Xin, ZHU Rui-fu, GAO Han, XU Wei-li, XIAO Gui-yong, CHEN Chuan-zhong, LU Yu-peng. A high bioactive alkali-treated titanium surface induced by induction heat treatment [J]. Surface and Coatings Technology, 2020, 385: 125362.

[198] SHAHRIYARI F, RAZAGHIAN A, TAGHIABADI R, PEIROVI A, AMINI A. Effect of friction hardening pre-treatment on increasing cytocompatibility of alkali heat-treated Ti−6Al−4V alloy [J]. Surface and Coatings Technology, 2018, 353: 148−157.

[199] ZHAO Xing-chuan, REN Xiao-jian, WANG Chang-zheng, HUANG Bao-xu, MA Jie, GE Bo, JIA Zheng-feng, LI Yu-chao. Enhancement of hydroxyapatite formation on titanium surface by alkali heat treatment combined with induction heating and acid etching [J]. Surface and Coatings Technology, 2020, 399: 126173.

[200] LEE B H, KIM Y D, SHIN J H, LEE K H. Surface modification by alkali and heat treatments in titanium alloys [J]. Journal of Biomedical Materials Research, 2002, 61(3): 466−473.

[201] ZHAO Guo-liang, XIA Long, ZHONG Bo, WU Song-song, SONG Liang, WEN Guang-wu. Effect of alkali treatments on apatite formation of microarc-oxidized coating on titanium alloy surface [J]. Transactions of Nonferrous Metals Society of China, 2015, 25(4): 1151−1157.

[202] PRASAD S, EHRENSBERGER M, GIBSON M P, KIM H, MONACO E A Jr. Biomaterial properties of titanium in dentistry [J]. Journal of Oral Biosciences, 2015, 57(4): 192−199.

[203] MOSSINO P. Some aspects in self-propagating high-temperature synthesis [J]. Ceramics International, 2004, 30(3): 311−332.

生物医用植入体钛基合金及其表面生物活性氧化层的制备：机遇与挑战

Mohamad Rodzi SITI NUR HAZWANI, Ling Xin LIM, Zainovia LOCKMAN, Hussain ZUHAILAWATI

Biomaterials Niche Area Group, School of Materials and Mineral Resources Engineering,
Universiti Sains Malaysia, Engineering Campus, 14300 Nibong Tebal, Penang, Malaysia

摘　要：钛及其合金因其优异的力学性能和良好的生物相容性，长期以来一直被用作植入材料。尽管如此，研究人员和行业仍在积极寻求更好的合金，因为仍有一些迫切的问题需要关注，包括：(1) 由于种植体材料与人体骨组织的弹性模量不匹配而导致的应力屏蔽问题；(2) Ti 合金长期使用后有害离子的释放问题；(3)钛合金表面生物活性低而导致愈合过程延长。为了解决这些问题，很多研究工作致力于寻找含有更强生物相容性相成分的新一代钛合金，并对其表面进行改性，使其从天然的生物惰性转变为生物活性。本文回顾了最近报道的钛合金制备方面的工作，并基于所做的调查，强调弹性模量和使用无毒金属元素来提高生物相容性的重要性。在钛合金的表面改性方面，大量研究发现在表面生长的纳米氧化层有利于提高钛合金的生物活性，使其在植入后能够快速修复组织。本文全面地综述并重点考察适合用于生物医用植入体新型钛合金的相和成分，并强调制备和表面改性方法。

关键词：钛合金；整形外科应用；表面改性；TiO_2 纳米管

(Edited by Xiang-qun LI)